N-glycosylation engineering in chimeric antigen receptor T cells enhances anti-tumor activity

Elien De Bousser[1,2,4*] & Nele Festjens[1,2,4*°], Evelyn Plets[1,2], Leander Meuris[1,2,4], Laura Vuylsteke[1,2], Daria Fijalkowska[1,2], Annelies Van Hecke[1,2], Elise Wyseure[1,2], Marie Goossens[1,2,4], Laure De Pryck[1,2,4], Sam Van den Bosch[1,2], Stijn De Munter[3,4], Bart Vandekerckhove[3,4], Nico Callewaert[1,2,4°]

[*]These authors contributed equally to this work

°Correspondence should be addressed to NF (Nele.Festjens@vib-ugent.be; https://orcid.org/0000-0002-3429-5463) and NC (Nico.Callewaert@vib-ugent.be; https://orcid.org/0000-0003-2069-6917).

[1]VIB Center for Medical Biotechnology, VIB, Ghent, Belgium
[2]Department for Biochemistry and Microbiology, Ghent University, Ghent, Belgium
Technologiepark-Zwijnaarde 75, 9052 Ghent, Belgium
[3]Department of Diagnostic Sciences, Ghent University, Ghent, Belgium
[4]Cancer Research Institute Ghent (CRIG), Ghent, Belgium

Author contributions:

Conceptualization: EDB, NF, NC
Methodology: EDB, NF, SDM, NC
Software: LM, DF
Validation: EDB, NF, LM, DF, NC
Formal analysis: EDB, NF, LM, DF, NC
Investigation: EDB, NF, EPL, LV, AVH, EW, MG, LDP, SVdB
Resources: EDB, NF, LM, DF, SDM, BV, NC
Data curation: EDB, NF, LM, DF, NC
Writing – original draft: EDB, NF, LM, DF, NC
Writing – review & editing: EDB, NF, NC
Visualization: EDB, NF
Supervision: EDB, NF, NC
Project administration: EDB, NF
Funding acquisition: EDB, NF, NC

Abstract

Chimeric antigen receptor (CAR) T cell therapy has had limited success in solid tumors, requiring novel enhancement strategies. Modifying the glycocalyx of CAR T cells is unexplored; we report on genome-editing of the *MGAT5* gene to abolish human CAR T N-glycan poly-LacNAc modifications. This boosted tumor control in carcinoma and lymphoma models, for donors of whom the non-engineered CAR T cells largely failed in tumor control. More blood-circulating MGAT5 KO CD70 nanoCAR T cells were found, exhibiting potent tumor cell-killing activity *ex vivo*, while non-glycoengineered CAR T cells faltered. MGAT5 KO CD70 nanoCAR T cells also mediated durable anti-tumor immunity, improving control of secondary carcinoma challenge months later. Single-cell transcriptomics revealed increased mitotic activity and type I interferon signaling, indicating sustained intratumoral activation. The glyco-engineered cells had unaltered antigen sensitivity and dependence on T cell growth factors, preserving key safety features. *MGAT5* KO is readily compatible with clinical manufacturing, representing a promising approach to enhance CAR T cell therapy.

48 ## Introduction

49 Immunotherapy with T cells that are genetically modified to express chimeric antigen receptors (CARs) has
50 shown impressive efficacy in many, but by no means all patients suffering from a range of hematological
51 malignancies[1–3]. The translation of this clinical success to a larger proportion of patients, and especially to
52 the treatment of solid tumors, requires to overcome multiple obstacles[4,5]. In general, robust and stable
53 populations of CAR T cells are required that are able to infiltrate the tumor and escape the
54 immunosuppressive effect of the tumor micro-environment (TME), and which install long-term functional
55 anti-tumor memory as to control also tumor relapses.

56 Whereas many aspects of T cell biology are being engineered to explore efficacy enhancement, the
57 complex glycocalyx at the CAR T cell surface that mediates initial contacts of cells with their environment
58 remains unexploited. However, basic research has revealed that surface glycosylation regulates important
59 aspects of T cell functionality. For example, the expression of immune checkpoint inhibitors such as PD-1
60 and CTLA-4 is tuned by glycosylation[6,7]. Selective removal of NXS/T N-glycosylation sites from the TCR also
61 enhances receptor diffusion, multimerization and functional avidity[8]. Furthermore, there is *in vitro*
62 evidence that β-galactoside binding lectins (incl. mammalian galectins) can have a strong impact on the
63 functionality of T cells. *Ex vivo* treatment of tumor-infiltrating T cells with an anti-galectin-3 antibody or a
64 galectin competitive binder such as N-acetyllactosamine (LacNAc) resulted in the detachment of surface
65 galectin-3, leading to increased cytotoxicity and ability to secrete cytokines such as IFN-γ[13,19]. Similarly,
66 galectin-9 binding to TIM-3 was associated with the promotion of $CD8^+$ T cell apoptosis[12,13]. On the other
67 hand, galectin-1 was observed to promote expansion of regulatory T cells (Tregs) and induces apoptosis of
68 specific thymocyte subsets and activated T cells, a process mediated at least in part through interaction
69 with glycans on CD45[14,15].

70 Inactivation experiments of the enzymes involved in the synthesis of poly-LacNAc structures corroborated
71 their importance in T cell regulation. β1,6-N-acetylglucosaminyltransferase-V (MGAT5) is the enzyme
72 responsible for the initiation of the GlcNAc-β-(1,6)-branch on N-glycans, which can be further elongated to
73 carry poly-LacNAc chains **(Figure 1.**A**)**. Absence of MGAT5, and thus a decrease in cell surface LacNAc
74 density, lowers murine T cell activation thresholds by enhancing TCR clustering due to reduced galectin-
75 glycoprotein lattice formation, which could be phenocopied *in vitro* by lactose addition to T cells[16].
76 Similarly, murine T cells mutated in β1,3-*N*-acetylglucosaminyltransferase (β3GnT2), which extends β1,6-
77 branched *N*-glycans with poly-*N*-acetyllactosamine, show a lower threshold for TCR activation[17] and
78 proliferated more strongly than their wild type counterparts. More recently, the *MGAT5* gene was found
79 as a key functionally validated hit in a CRISPR screen for enhanced intratumoral $CD8^+$ T cell numbers in a
80 murine model of glioblastoma[18]. With cessation of T cell responses, surface levels of the adhesion receptor

81 cytotoxic T-lymphocyte antigen (CTLA-4) increase, a process dependent on increases in both CTLA-4 gene
82 expression and MGAT5-mediated N-glycan branching[7]. Higher surface levels of CTLA-4 oppose CD28-
83 dependent adhesion to CD86/CD80 on antigen-presenting cells, functioning as an immune checkpoint[19].
84 Furthermore, negative regulation of TCR signaling by β1,6-GlcNAc-containing N-glycans promotes
85 development of Th2 over Th1 responses, enhancing Th2 polarization[20]. Moreover, *MGAT5* expression can
86 be induced by the cytokine IL-10, decreasing antigen sensitivity of $CD8^+$ T cells[21]. Many of these processes
87 are involved in the immunosuppressive micro-environment of tumors. Accordingly, systemic inhibition in
88 mice of the biosynthesis of LacNAc glycans via administration of a cell-membrane permeable enzyme
89 inhibitor increased the number of infiltrating tumor-specific T cells[22], as did administration of a
90 polysaccharide with galectin-displacing properties[22,23].

91 Taken together, these fundamental immune-glycobiological study data gathered over two decades from
92 multiple labs on poly-LacNAc modifications on T cells, indicated that poly-LacNAc modification in the T cell
93 glycocalyx may function as a multipronged checkpoint mechanism that limits antitumor T cell immunity.
94 Glycobiology can be notoriously difficult to translate from murine studies to humans, as qualitative and
95 quantitative aspects of the outer branch modifications of the glycocalyx are amongst the most rapidly
96 evolving mammalian cellular structures, likely under differential pathogen pressure[24]. Whether sufficient
97 aspects of the mainly murine T cell based glycobiology described above would be applicable to human CAR
98 T cells, with their independence from TCR-antigen recognition and the intricacies of TCR-coreceptor
99 clustering, was unexplored. Hence, we set out to test the hypothesis whether genetic inactivation of poly-
100 LacNAc N-glycan biosynthesis in human CAR T cells by *MGAT5* gene inactivation would lead to more
101 efficacious treatment of human lymphoma and carcinoma tumor models. These studies are the first to
102 report on targeting of the glycocalyx of CAR T cells for therapy enhancement.

103 Results

104 Generating MGAT5 knockout (KO) CD70 nanoCAR T cells

105 Staying close to the currently used methods for human CAR T cell therapy manufacturing, we optimized a
106 workflow for the combined CRISPR-Cas9 mediated *MGAT5* mutagenesis and retroviral CAR delivery to
107 purified, activated human $CD3^+$ T cells (**Figure 1**.B and **Supplementary Figure 2**). The presence of both $CD4^+$
108 and $CD8^+$ T cell subsets in the final CAR T cell product is indispensable for efficient anti-tumor immunity[25].
109 The mean editing efficiency as percentage insertions and deletions (% indel) for the *MGAT5* locus over
110 multiple (n=26) experiments was consistently high (exceeding 80% indel) as is depicted in **Figure 1**.C. Flow
111 cytometry was used to measure both CD70 nanoCAR expression and GFP expression as readouts of the
112 retroviral transduction efficiency[26]. CD70 nanoCAR transduction efficiencies of more than 70% were
113 consistently obtained over multiple (n=26) experiments, irrespective of whether the *MGAT5* gene was
114 engineered or not (**Figure 1**.D).

115 **MGAT5 KO CD70 nanoCAR T cells have strongly reduced N-glycan poly-LacNAc cell surface density**

116 In order to assess the extent of the intended reduction in poly-LacNAc cell surface abundance, we used
117 flow cytometry to measure binding of the lectin from *Datura stramonium* (DSL) (**Figure 1**.E). This lectin
118 binds to all glycans containing (poly-)LacNAc glycotopes regardless of whether they are linked to N-glycans,
119 O-glycans or glycosphingolipids. MGAT5 KO CD70 nanoCAR T cells had about 50% reduced staining with
120 DSL. Furthermore, using the lectin from *Phaseolus vulgaris* (PHA-L), which specifically binds to N-glycans
121 carrying the MGAT5-synthesized β-1,6 branch, we observed near-complete loss of binding (**Figure 1**.E).
122 Together, these results show that the extent of *MGAT5* genome editing efficiency that we achieved
123 successfully eliminates N-glycan β1,6-branching. The loss of β-1,6 branch formation on the N-glycans was
124 corroborated by direct structural profiling of the N-glycans shaved off the cell surface using PNGase F
125 enzyme, followed by capillary gel electrophoresis with laser induced fluorescence (CGE-LIF) (**Figure 1**.F), a
126 method previously developed at our lab[27,28]. The desialylated N-glycan profile of MGAT5 KO CD70 nanoCAR
127 T cells demonstrates a loss of the main tetra-antennary N-glycan species (synthesis of which requires
128 MGAT5), whereas the tri-antennary precursor N-glycans that MGAT5 takes as its substrates are increased
129 in relative abundance, as expected.

130 **MGAT5 KO CD70 nanoCAR T cells are fully functional *in vitro* and expand more upon repeated tumor cell**
131 **challenge**

132 MGAT5 KO CD70 nanoCAR T cells have equivalent viability rates as non-glycoengineered control cells *in*
133 *vitro* (**Figure 1**.G). After CAR construct transduction and subsequent cultivation, most of the CAR T cells in
134 the total $CD3^+$ T cell pool are $CD4^+$, and this was even more pronounced when CD70 nanoCAR T cells
135 underwent CRISPR-Cas9 engineering (both for mock gRNA and *MGAT5* KO gRNA), generating a CAR T cell
136 preparation with about 80% $CD4^+$ and 20% $CD8^+$ (**Figure 1**.H). Using flow cytometrical methods, we
137 quantified production proficiency for the TNF-α, IFN-γ and IL-2 cytokines of the glyco-engineered CD70
138 nanoCAR T cells, after challenging them with the THP-1 and SKOV-3 target tumor cell lines (**Figure 1**.I-K). At
139 least as high a proportion of the MGAT5 KO CD70 nanoCAR T cells are able to produce cytokines upon
140 antigen stimulation as are mock-nucleofected CD70 nanoCAR T cells. This cytokine expression is dependent
141 on CD70 nanoCAR expression, given that the fraction of cytokine-expressing non-transduced T cells (NTC)
142 is close to zero or very low in the presence of CD70 positive THP-1 cells (but high after polyclonal
143 Immunocult stimulation). In order to evaluate the combined proliferative and cytotoxic potential of MGAT5
144 KO CD70 nanoCAR T cells, very low proportions of CAR T cells were co-cultured with THP-1 target cells. The
145 number of THP-1 cells left surviving in culture was determined by flow cytometry. At day 7, a second
146 challenge with target THP-1 cells was performed. **Figure 1**.L and N show the results corresponding to an
147 effector/target (E/T) ratio of 0.15 and 0.015. At these ratios, all target cells get killed by day 4, in all of the
148 mock-nucleofected and MGAT5 KO CD70 nanoCAR T cell conditions. Interestingly, upon second challenge

149 with tumor cells, at both E/T ratios, the number of CD70 nanoCAR T cells is significantly higher for those
150 that are KO in *MGAT5*, indicating a stronger and more sustained antigen recognition-induced expansion of
151 these glyco-engineered CAR T cells (**Figure 1**.M and O).

152 **Treatment of carcinoma-bearing mice with MGAT5 KO CD70 nanoCAR T cells yields improved tumor control**
153 A key challenge with translationally relevant CAR T cell studies using human donor cells in preclinical mouse
154 models is the substantial observed biological variability from donor to donor in the derived baseline CAR T
155 cell potency[29–31], varying from complete tumor control to barely any tumor control, which is also observed
156 in the clinic. Hence, also our studies aimed at realistically preclinically evaluating human CAR T MGAT5
157 engineering in human tumor xenograft mouse models. This required a significant experimental effort to
158 obtain a representative picture of the spectrum of effect sizes of the *MGAT5* KO engineering, observed
159 over 3 or 4 donors each time.

160 As CAR T cell therapy clinically so far mostly fails in carcinomas and improvements there would open
161 exciting translational opportunities, we chose to first test experimental therapeutic efficacy of the MGAT5
162 KO CD70 nanoCAR T cells in the NSG[32] mouse xenografted with CD70-expressing SKOV-3 ovarium
163 carcinoma cells, the latter engineered to produce luciferase, for longitudinal tumor burden measurement.
164 These tumors establish a micro-environment in which most of the known T cell immunosuppressive
165 mechanisms are at play, thus forming a truly challenging target for CAR T therapy[33–36]. The experimental
166 layout is illustrated in **Figure 2**.A and runs for 120 days, including primary tumor challenge and relapse-
167 mimicking secondary tumor challenge in surviving mice, to assess long-term functional persistence of CAR
168 T cells. Full time-course results were obtained for three independent experiments, performed with T cells
169 from different donors (Donor A, B and C). The outcome of treatment for the primary tumor was categorized
170 as: (1) full control, i.e. the tumor becomes undetectable and no relapse follows; (2) full control but
171 occurrence of a relapse later on; (3) partial control, i.e. a halt in tumor growth but the tumor remains
172 detectable; (4) no control of tumor growth throughout the duration of the experiment.
173 As is clear from **Figure 2**.B and the bar graphs in **Figure 2**.C, in this model the primary tumor is never
174 controlled by the mice that did not receive CAR T cells; they were all sacrificed at the humane endpoint. A
175 considerable number of mice (n=19) in the non-glycoengineered CAR T cell treated groups across the 3
176 donors show only partial or even no control at all of the primary tumor, while this was the case for only 9
177 mice in the MGAT5 KO groups.

178 Donor A represents the case in which potent CAR T cells can be obtained without any further engineering:
179 even the non-glycoengineered CAR T cells were fully efficacious at controlling the primary tumor and we
180 did not observe any relapse at the primary tumor site over time (**Figure 2**.B and **Supplementary Figure 4**.A-
181 B). Donors B and C represent the clinically more frequently observed picture where CAR T cells have

182 variable and generally low capacity of clearing carcinoma. For both donors, MGAT5 KO CD70 nanoCAR T
183 treatment led to significantly improved primary tumor control compared to treatment with non-
184 engineered CD70 nanoCAR T cells (**Supplementary Figure 5**.A-B and **Supplementary Figure 6**.A-B). However,
185 for these donors the primary tumor regrew even when it was initially cleared (**Figure 2**.B). Using the data
186 for these two donors where relapses were observed, a Kaplan-Meier survival analysis detected that a
187 longer relapse-free survival was obtained in the MGAT5 KO CD70 nanoCAR T treated groups
188 (**Supplementary Figure 3**.A-B).

189 To test for long-term functional persistence of the CAR T cells and capability of mounting a functional anti-
190 tumor response, we mimicked a relapse tumor after a period of approximately 90 days, by rechallenge
191 with a secondary tumor in the opposite (left) flank of the CAR T treated mice that survived the primary
192 tumor. For this secondary tumor, we defined four types of tumor control: (1) no tumor, meaning the
193 secondary tumor never develops; (2) full control, i.e. the secondary tumor becomes undetectable after an
194 initial growth phase; (3) partial control, i.e. the secondary tumor stops growing but remains detectable; (4)
195 no control of secondary tumor growth throughout the duration of the experiment. In order to have a
196 control group (untreated) with comparable age and history as the remaining mice from the treatment
197 arms, we tumor-challenged a group of mice that were kept in husbandry from the very start of the
198 experiment but that did not receive a primary tumor challenge. As shown in **Figure 2**.B and the bar graph
199 in **Figure 2**.D, MGAT5 KO CD70 nanoCAR T cell treatment also leads to better rechallenge tumor control. In
200 the experiment with CAR T cells from donor A, the average tumor volume at the end of the analysis is an
201 estimated 6.4 times smaller (p=0.011) in mice that were treated with MGAT5 KO CD70 nanoCAR T cells
202 compared to non-glycoengineered CAR T treated mice (**Supplementary Figure 4**.C-D). For those mice
203 treated with CAR T cells from donor B that still had a remnant of the primary tumor at the timepoint of
204 rechallenge, we found that at the end of the experiment, these tumors had a smaller average size in the
205 MGAT5 KO group than in the non-glycoengineered CAR T cell treated group, although the difference was
206 not statistically significant (**Figure 2**.B, **Supplementary Figure 5**.C-D).

207 Hence, we concluded that in all analyses where non-engineered donor CAR T cells did not or partially
208 control the tumors, their MGAT5 KO-engineered counterparts substantially rescued this.

209 **When MGAT5 KO enhances primary tumor control, higher numbers of MGAT5 KO CD70 nanoCAR T cells are**
210 **present in blood as compared to non-glycoengineered CD70 nanoCAR T cells**

211 We quantified the number of circulating human $CD3^+$ T cells and the CAR-engineered subpopulation
212 thereof in blood. We first sampled blood on day 34, which is 21 days after CAR T cell administration. At this
213 timepoint, the spectrum of donor-dependent variance in therapeutic response is first clearly detected,
214 (**Figure 2**.B, left panels), making it a suitable timing to measure the strength of the CAR T proliferation.

215 Interestingly, for the two donors (B and C) whose non-glycoengineered CAR T cells did not completely
216 control the tumor and where MGAT5 KO CD70 nanoCAR T cells yielded substantial tumor control
217 enhancement, the number of MGAT5 KO CD70 nanoCAR T cells in blood (**Figure 2.**E, left panels) is
218 significantly increased as compared to the counterpart non-glycoengineered CD70 nanoCAR T cells. In
219 contrast, for donor A, whose CAR T cells completely eradicated the tumor already without glyco-
220 engineering, even higher numbers of CAR T cells were present already for non-engineered CAR T cells and
221 this number was not further boosted by *MGAT5* KO engineering. It is also striking that in donor C, where
222 CAR T therapy was the least successful, also the lowest average number of CAR T cells amongst the 3 donors
223 are found. *MGAT5* KO boosts this significantly leading to strongly enhanced survival of the challenged mice
224 (at day 84 just prior to second tumor challenge: 13 out of 14 surviving for MGAT5 KO CD70 nanoCAR T vs.
225 7 out of 13 for non-glycoengineered CAR T), with 10 also surviving secondary tumor challenge, whereas
226 only 3 mice were still alive in the non-glycoengineered CAR T treated group at the end of the experiment.
227 Donor B is intermediate between A and C and indeed also had intermediate levels of circulating non-
228 engineered CAR T cells. The *MGAT5* KO boost of this donor's CAR T cells was here sufficient to get all
229 primary tumors cleared initially, with full survival (9 out of 9 mice) till day 90 (when we performed tumor
230 rechallenge), whereas by this timepoint we lost 1/3rd of the mice treated with non-engineered CAR T cells
231 (12 out of 18 surviving). Hence, this exploration revealed that there is a striking correspondence between
232 the increased blood concentration of CAR T cells and the tumor control success.
233 Blood sampling was repeated around day 80 (i.e. shortly prior to tumor rechallenge) and at the end of the
234 experiments on days 118-123 (which is about 35 days after the tumor rechallenge), at which time also the
235 spleen CAR T cell counts of all mice surviving up to that point were measured. At the late timepoint prior
236 to tumor rechallenge (day 80), a more than 10-fold contraction of the concentration of CAR T cells was
237 observed for donor A (**Figure 2.**E, compare right and middle panels) where no tumor had been present for
238 about 2 months, as one would expect in the absence of CAR antigen. In donor B, such contraction was only
239 observed for the MGAT5 KO group and to a lesser extent than in donor A; this is in line with the observation
240 that this group had cleared the tumor initially, but very small tumors slowly regrew, providing some
241 antigenic stimulation. In contrast, the CAR T numbers in the group treated with non-engineered donor B
242 CAR T cells did not contract, in accordance with most surviving mice never having cleared their tumor over
243 this time course, providing continuous antigenic stimulation. The same was seen in donor C, here both for
244 the non-glycoengineered CAR T group and for the MGAT5 KO CD70 nanoCAR T group, in line with
245 continuous tumor exposure in the mice.
246 Upon tumor rechallenge (**Figure 2.**E, compare middle and right panels) no major differences occurred in
247 donor B, whereas in donor A, MGAT5 KO CD70 nanoCAR T blood cell concentration appeared to somewhat
248 re-expand by this renewed antigen stimulation vs. a further mild contraction observed for non-glyco-

249 engineered cells, with the MGAT5 KO treated group indeed achieving better secondary tumor control
250 (**Figure 2**.B, right panels). It must be noted that all of these median levels for donor A and donor B are still
251 around or above 1000 CAR T cells per ml of blood, which also at the day 34 timepoint appears to be close
252 to the threshold needed to achieve SKOV-3 tumor control. Remarkably, for donor C, rechallenge with the
253 tumor also leads to further expansion of the MGAT5 KO CD70 nanoCAR T cells, to the levels seen to robustly
254 eliminate tumor cells in the other donors. However, no differences could be observed in terms of tumor
255 killing (**Supplementary Figure 6**.C-D).
256 For the experiment with donor A in which the primary tumor was completely cleared, also with non-
257 glycoengineered CAR T cells, we sacrificed half of the mice at day 34 in order to investigate spleen CAR T
258 counts at that early timepoint as well. Remarkably, the number of MGAT5 KO CD70 nanoCAR T cells in the
259 spleen was higher in these mice vs. the non-glycoengineered CAR T cells (**Figure 2**.F), and the numbers
260 were extremely high (median above 100,000 CAR T cells per spleen for the MGAT5 KO group). Investigating
261 the spleens at the end of the experiments, there were no longer differences in CAR T cell numbers between
262 MGAT5 KO and non-glycoengineered groups, for all donors, and the numbers were much lower, close to
263 background for donor A, intermediate for donor B and highest for donor C (medians not exceeding 10,000
264 cells per spleen).

265 **MGAT5 KO CD70 nanoCAR T cells enhance control of a highly aggressive metastatic B cell lymphoma model**
266 To investigate the scope of applicability of the MGAT5 KO engineering module, we have expanded our
267 findings to a very different tumor type, i.e. the Non-Hodgkin B cell lymphoma setting in which CAR T therapy
268 is already part of the standard of care treatment paradigm, but where efficacy enhancement is still also
269 sorely needed. In contrast to the localized subcutaneous SKOV-3 tumor, in this case NSG mice were
270 intravenously injected with luciferase-expressing Raji cells, resulting in a metastatic model that establishes
271 a very rapidly growing multi-systemic human lymphoma burden, incl. in the brain[37]. This forms a stringent
272 test for CAR T cell therapy, as therapeutic cells need to exert tumor control very rapidly, which leads to
273 terminal tumor burden in all mice within 1 week after the treatment timepoint when left untreated. This
274 is translationally reminiscent of the clinical setting of treating patients with relapsing lymphoma. Raji
275 lymphoma also expresses the CD70 antigen (**Supplementary Figure 1**), which is an emerging new target
276 antigen in both B and T cell lymphomas also clinically[38,39], so we could use the same nanoCAR against CD70
277 that we used for the above SKOV-3 carcinoma work, allowing for comparison of the results. Seven days
278 after tumor cell inoculation, mice were treated with either mock Cas9-engineered or MGAT5 KO CD70
279 nanoCAR T cells. As control groups, mice were treated with non-transduced T cells to evaluate tumor
280 development. Throughout the experiment, tumor burden was measured by bioluminescence imaging (BLI).
281 A schematic representation of the experimental timeline is depicted in **Figure 3.**A. The experiment has been
282 repeated on four different donors (donor D, E, F, G), in order to be able to take into consideration the

283 variability in the efficacy of CAR T cells derived from different donors. For two out of four donors (F and G)
284 we found that *MGAT5* KO leads to a >50% enhanced long-term survival rate (**Figure 3**.B), with monitoring
285 in all experiments for at least 90 days post-tumor challenge. As with the SKOV-3 carcinoma model, again
286 we observed that in these two donors where MGAT5 KO resulted in the biggest enhancement vs. mock-
287 engineered CAR T cells, a significantly higher number of MGAT5 KO CD70 nanoCAR T cells were found in
288 the blood at the early timepoint 2 weeks after CAR T treatment (**Figure 3**.C). In most of these long-term
289 surviving mice, the tumor became undetectable (**Figure 3**.B-C, right panels), a truly remarkable result given
290 the extreme aggressivity of this tumor model. For donor E, the non-engineered CAR T cells already yielded
291 survival of 3 out of 4 mice, and MGAT5 KO turned this into complete protection (4/4). Here, we also found
292 a trend to higher numbers of MGAT5 KO CD70 nanoCAR T cells in the blood. In donor D, neither non-
293 engineered nor MGAT5 KO CD70 nanoCAR T cells yielded any long-term survival. This donor's cells were
294 an outlier, with massive CAR T cell proliferation, yielding cell numbers at least 10-fold higher than in any of
295 our other experiments. It appears that these donor's CAR T cells are extraordinarily stimulated to
296 proliferate, yet defective in tumor killing capacity.

297 In conclusion, MGAT5 KO substantially enhanced the protective capacity of CD70 nanoCAR T cells in the
298 metastatic Raji lymphoma model, concomitant with enhanced concentration of CAR T cells in the blood,
299 therewith corroborating the results obtained in the SKOV-3 model as described above.

300 **The higher number of circulating MGAT5 KO nanoCAR T cells results in higher *ex vivo* tumor cell killing activity**
301 **over prolonged tumor cell challenge.**
302 From these findings, the simplest conceivable mechanism of action of the MGAT5 KO-mediated CAR T cell
303 enhancement was a higher and/or more prolonged circulating therapeutic cell level available to combat
304 tumor growth, resulting from stronger proliferation and/or from stronger tumor cell killing potency of the
305 CAR T cells. For this, it was necessary to investigate whether this enhanced concentration of circulating
306 MGAT5 KO CD70 nanoCAR T cells in blood is indeed competent by itself at more effectively killing tumor
307 cells *ex vivo* (**Figure 4**). Hereto, we prepared blood from SKOV-3 tumor-bearing mice 21 days after
308 treatment with either non-glycoengineered CD70 nanoCAR T cells versus MGAT5 KO CD70 nanoCAR T cells
309 from 2 extra independent donors (donor H/I) (**Figure 4**.A). For donor H, SKOV-3 tumor stasis was achieved
310 in the mice in the MGAT5 KO CD70 nanoCAR T treated group, while this was not the case for the mock
311 CD70 nanoCAR T treated group (**Figure 4**.B), similar to the case of donor C described above (**Figure 2**). For
312 donor I, the MGAT5 KO and mock engineered CD70 nanoCART cells both completely cleared the tumor
313 (**Figure 4**.F), similar to donor A above (**Figure 2**). In both cases, higher numbers of MGAT5 KO CD70 nanoCAR
314 T cells were again detected (**Figure 4**.C and G). To investigate whether this resulted in higher tumor cell
315 killing activity per volume of blood, cells prepared from equivalent volumes of blood were co-cultured with
316 THP-1 tumor cells (which are CD70 expressing suspension cells and thus more amenable to this co-culture

317 analysis than SKOV-3) at different ratios, and THP-1 cell counts as well as CAR T counts were followed over
318 time. **Figure 4**.D shows that circulating MGAT5 KO CD70 nanoCAR T cells from donor H efficiently and
319 almost completely wiped out the THP-1 tumor cells, even upon a second THP-1 tumor cell challenge at day
320 7, whereas blood cells from the non-glyco-engineered CAR T treated mice were ineffective at controlling
321 the THP-1 cells even in the first round of challenge. Circulating non-glyco-engineered CAR T cells from
322 donor I showed delayed control of THP-1 cells compared to MGAT5 KO CD70 nanoCAR T cells (**Figure 4**.H),
323 with viable THP-1 cells still observed at day 4 of co-culture, whereas at day 7 both blood-derived CAR T
324 preparations had cleared the tumor cells. There was no control of THP-1 target cells when using blood cells
325 from mice treated with non-engineered T cells from the same donors. Moreover, MGAT5 KO CD70
326 nanoCAR T cells from both donors proliferated much stronger than non-engineered counterparts in these
327 *ex vivo* co-cultures, and in both cases sustained this also after the second THP-1 cell addition (**Figure 4**.E
328 and I). Hence, we conclude that MGAT5 KO results in a higher level of tumor cell killing-competent CAR T
329 cells surveilling the body of the CAR T treated mice, with these cells remaining cytotoxic and proliferating
330 also after prolonged tumor cell encounter, providing a simple mechanism for the enhanced observed *in*
331 *vivo* tumor control.

332 **MGAT5 KO CD70 nanoCAR T cells require equal antigen density to degranulate and remain fully dependent**
333 **on cytokine growth factors for their proliferation.**

334 Beyond elevated concentrations of circulating CAR T cells with persistent tumor cell killing competence,
335 another conceivable mechanism of action for MGAT5 KO in enhancing antitumoral potency could be a
336 lowered threshold of antigen density required for CAR T cell activation. To investigate this, we have
337 analyzed degranulation levels (using the CD107a/LAMP1 exposure on the cell membrane as a proxy) in
338 function of incubation of CAR T cells on varying concentrations of coated recombinant human CD70
339 antigen. We find similar activation thresholds for non-glycoengineered versus MGAT5 KO CD70 nanoCAR
340 T cells, indicating that increased tumor cell control of MGAT5 KO CD70 nanoCAR T cells is not due to a
341 decreased activation threshold, which otherwise may increase the risk for overstimulation or off-target
342 activation (**Figure 5**.A).

343 Furthermore, in the absence of antigen, neither mock nor MGAT5 KO CD70 nanoCAR T cells grow without
344 IL-7/IL-15 (growth/survival-associated cytokines) (**Figure 5**.B), demonstrating that these nanoCAR T cells
345 are still signal-3 dependent and not transformed, a key safety requirement. Together, the data indicate
346 that MGAT5 KO CD70 nanoCAR T cells retain an inherent capacity for more vigorous and prolonged antigen-
347 and cytokine-dependent proliferation without making the cells hypersensitive to antigen.

348 Furthermore, we did not observe any signs of graft-versus-host-disease (GvHD) in any of the SKOV-3 *in vivo*
349 experiments with 5 human donors. In the Raji model, in which CAR T cells proliferate to much higher

350 numbers than in the SKOV-3 model, we observed signs of GvHD in 1 out of 22 mice in the non-
351 glycoengineered CAR T treatment groups across the 4 donor experiments, and in 3 out of 19 mice in the
352 MGAT5 KO nanoCAR T treatment groups.

353 **MGAT5 KO enhances type I IFN signaling and other hallmarks of enhanced persistent activation and**
354 **proliferation in tumor-infiltrating CAR T cells**

355 What remained was to explore which alterations were present in the state of MGAT5 KO tumor-infiltrating
356 nanoCAR T cells. To this effect, 10 days after SKOV-3 tumor inoculation, we treated groups of 6 mice with
357 CD70 nanoCAR T cells and after 7 days we collected peripheral blood and resected the tumors. CAR T cells
358 were sorted from these samples and we performed single-cell RNA sequencing (scRNAseq) (**Figure 6**.A). As
359 can be seen in **Figure 6**.B, this timepoint 17 days post-tumor inoculation is a few days before we start
360 measuring tumor size divergence between non-glycoengineered and MGAT5 KO CD70 nanoCAR T cell
361 treated mice, and was chosen as it should allow for the most unbiased sampling of initial tumor attack.
362 Uniform manifold approximation and projection (UMAP) analysis of the single cell transcriptomes revealed
363 that tumor-infiltrating CAR T cells were clearly distinguished from those circulating in blood (**Figure 6**.B).
364 CAR T cells separated further into $CD4^+$ and $CD8^+$ populations (**Figure 6**.C). In blood, cell cycle stage
365 inference from RNA expression profiles revealed a large stationary population and a small proliferating
366 population of CAR T cells (**Figure 6**.D). Compared to circulating cells, CAR T cells from tumor were generally
367 in a more activated, proliferative state, with a gradient-like separation of predicted cell cycle phases (**Figure**
368 **6**.D).

369 Based on CD4/CD8 state, blood/intratumoral location and inferred cell cycle phases, we defined 7 clusters
370 (Figure 6.E) for further exploration of transcriptional differences associated with MGAT5 KO. Subsequently,
371 differential expression (DE) analysis was performed within the same cluster, revealing a total of 193
372 significant DE genes between MGAT5 KO and non-glycoengineered in at least one of the clusters (Wilcoxon
373 Rank Sum test for genes expressed in at least 25% of cells of one of the compared populations and minimal
374 fold change threshold of 0.1, Bonferroni-corrected p-value of at least 0.05; Supplementary Table 1 We also
375 performed gene set enrichment analysis of Reactome pathways to perform the differential analysis at
376 functional pathway/module level (**Supplementary Table 2**), visualized according to statistical significance
377 level, fraction of pathway genes differentially regulated and mean log2 fold change of gene expression of
378 pathway genes in **Figure 6.**F[40]. The Reactome pathways related to active cell cycle progression were more
379 prominently upregulated in MGAT5 KO cells, whereas for the $CD4^+$ subfraction, we observed more
380 significant upregulation in MGAT5 KO cells of ribosomal biogenesis and translation, a known hallmark of
381 $CD4^+$ cell activation[41] (**Figure 6.**F). A somewhat higher proportion of active cell cycling (in G2M and S phase)
382 was observed in both the intratumoral $CD4^+$ and $CD8^+$ subfraction (**Supplementary Figure 7**.A).
383 Furthermore, across both $CD4^+$ and $CD8^+$ intratumoral fractions, strikingly, pathways related to IFN type I

384 signaling were significantly more activated upon MGAT5 KO in both CD4$^+$ and CD8$^+$ CAR T cells (**Figure 6**.F
385 and G), a feature of persistently activated T cells which we discuss further below as it is a topic of significant
386 current interest in CAR T cell enhancement-engineering. In blood, transcriptional differences were minor
387 between MGAT5 KO and non-glycoengineered cells, barely reaching statistical significance (**Supplementary**
388 **Figure 7**.B). The overall picture that emerges is that of MGAT5 KO CD70 nanoCAR T cells more vigorously
389 mounting a sustained proliferative cytotoxic antitumoral response through both a CD4$^+$ and a CD8$^+$ T cell
390 contribution, so it was interesting to compare our data with the transcriptional signature previously
391 reported for human CAR T cell exhaustion by prolonged antigen exposure[42]. Remarkably, MGAT5 KO
392 indeed significantly suppressed the gene signature associated with CAR T cell exhaustion by long antigen
393 exposure (**Figure 6.**H and I).

394 Discussion

395 The engineering of glycosylation in order to enhance biopharmaceutical functionality has met with
396 previous successes. The most notable example in the area of cancer immunotherapy is the discovery that
397 antibody dependent cellular toxicity potency of hIgG monoclonal antibodies could be boosted by
398 engineering of the production cell lines in various ways to reduce or abolish core-α-1,6-fucosylation of the
399 conserved CH2-domain linked N-glycan[43–45]. The strongly enhanced affinity to FcγRIIIa achieved in this way
400 is now at the basis of multiple enhanced anti-tumor antibody therapies[46–49]. The mammalian cell glycocalyx
401 constitutes a complex array of precisely regulated carbohydrate structures on transmembrane and
402 secreted proteins as well as on plasma membrane glycolipids. These glycans are biosynthesized in the cell's
403 secretory system by an array of glycosyltransferases and glycosidases. Cellular differentiation pathways as
404 well as cellular physiology alterations often result in cell-type and cell-state-specific glycocalyx composition
405 differences. This modulates altered interactions with the cellular environment, resulting in more or less
406 cell motility, adhesion, shaping of growth factor gradients, signaling receptor clustering at the cell surface
407 etc. In principle, this should offer novel biopharmaceutical opportunities for altering complex behavior of
408 therapeutic cells. This was the rationale for us to systematically start exploring the 'deconstruction' of the
409 CAR T cell glycocalyx through genome editing of glycosyltransferases that are at key positions in the glycan
410 biosynthetic pathways, and we here report on the first therapeutically relevant results from these ongoing
411 studies.

412 Poly-N-acetyllactosamine repeat structures occur on both N-and O-glycans of glycoproteins and on certain
413 glycosphingolipids. In human T cells, a large fraction is present on N-glycans, as staining with a lectin for
414 poly-LacNAc was reduced by >50% in our MGAT5 KO cells, which is why we prioritized studying N-glycan
415 poly-LacNAcylation for our studies. As reviewed in the introduction, basic immunology studies over the
416 past few decades, mainly in the mouse, also provided incentive to explore whether MGAT5 inactivation

417 would result in enhanced CAR T cell efficacy. However, promising basic immunology research findings on
418 T cell function in murine model cells do not necessarily translate to technologically useful interventions in
419 CAR T therapy. Hence, to ensure translational relevance of our results, we decided to stick as close as
420 possible to current human CAR T cell manufacturing methods for our studies. We coped with the well-
421 known large variance in quality of CAR T cells produced from different individuals by replicating the
422 laborious tumor control studies in mice with up to 5 human donors per tumor model. We used a highly
423 immunosuppressive human xenograft carcinoma model (SKOV-3) and a very aggressive model of
424 metastatic B cell lymphoma (Raji) to truly put our engineered CAR T cells to challenging tests that reflect
425 the 2nd or 3rd line tumor treatment setting in which CAR T cells are mostly used.

426 In summary, our data demonstrate that MGAT5 KO has the potential to enhance control of both carcinoma
427 and lymphoma tumors, through sustained elevated tumor cell-killing functionality and proliferation.
428 Especially when CAR T cells of human donors showed poor tumor control, MGAT5 KO boosted this
429 substantially and consistently. This was hallmarked by higher levels of active tumor cell-killing competent
430 CAR T cells in the systemic circulation, persistently constituting effective antitumor 'immune memory' that
431 could control secondary tumor challenges. These easy to monitor enhanced blood counts of MGAT5 KO
432 CD70 nanoCAR T cells, especially ~21 days post CAR T treatment, could constitute a convenient surrogate
433 biomarker for use in translation of our findings to clinical studies. MGAT5 KO does not enhance CAR T cell
434 antigen sensitivity (which may be in contrast to MGAT5 KO effect on TCR-mediated antigen recognition),
435 which we consider as favorable from a safety perspective, as many tumor-associated antigens are also
436 expressed at lower levels on healthy cells[16,20]. Also supporting the safety profile of the MGAT5 KO
437 intervention, the enhanced antigen recognition-triggered proliferation of MGAT5 KO cells is not because
438 of independence from cytokine growth factors, as the cells do not grow at all when these growth factors
439 are withdrawn.

440 The mild but comprehensive upregulation of type I interferon stimulated genes in MGAT5 KO CD70
441 nanoCAR T cells infiltrating the tumor suggests enhanced immune surveillance activity, a more
442 inflammatory or cytotoxic phenotype and could potentially be linked to persistent functional activation[50–
443 53]. Comparison of our single cell dataset of intratumoral CAR T cells to published data from a study
444 evaluating the response of T cells to continuous antigen exposure-triggered exhaustion, shows that the
445 gene expression signature linked to exhaustion is indeed suppressed in MGAT5 KO CD70 nanoCAR T cells[42].
446 Whereas type I interferon signaling is critical in activating and polarizing acute immune responses (most
447 studied in antiviral immunity), strong prolonged signaling dampens T cell activity upon prolonged antigen
448 stimulation such as in chronic viral infections[54,55]. Given this duality, how to intervene optimally in type I
449 interferon signaling to enhance CAR T therapy is not unequivocal in the literature[56–59]. Most studies that
450 completely inactivate type I interferon signaling have observed a level of enhanced CAR T potency, but a

451 very recent preprint publication reveals that strength of the type I interferon signal matters: with low but
452 not high concentrations of interferon-alpha addition during CAR T cell expansion, a more efficacious tumor
453 control was achieved[60]. We propose that our findings on mild type I interferon activation in intratumoral
454 MGAT5 KO CD70 nanoCAR T cells are consistent with this study, usefully achieving this phenotype after the
455 CAR T cells arrive in the tumor, when they are required to persistently activate in order to successfully
456 control the tumor.

457 Ensuring the technical feasibility of translating our findings to clinical CAR T production, we have
458 implemented MGAT5 KO by adding a CRISPR-Cas9 ribonucleoprotein nucleofection step to the standard
459 workflow that is already used for CAR T manufacturing in the clinic[61–63], and other preferred technologies
460 could likely be used for this as well[64–67]. It should hence be straightforward to plug in the MGAT5 KO module
461 onto most of the production workflows for almost any CAR T product.

462 Overcoming the poor proliferation and persistence of CAR T cells during solid tumor therapy, which results
463 in therapeutic failure, is a key and very active focus of research at the present time. Other promising
464 recently reported approaches involve installing autocrine cytokine production in the cells or ablating
465 immune signaling-dampening factors, in particular CD5[68–70]. We propose that CAR T cell surface poly-
466 LacNAc density reduction through inactivation of MGAT5 glycosyltransferase offers a novel highly
467 promising engineering module that targets the glycocalyx of the cells, a very different aspect of T cell
468 biology that remained unexplored as a CAR T engineering target until now.

469 Materials and methods

470 Ethical approval

471 Research work with anonymized buffy coats has been approved by the Red Cross Flanders (RKOV_19015,
472 G20240913A). All experiments were approved and performed according to the guidelines of the ethical
473 committee on Medical Ethics of Ghent University, Belgium (EC UZG 2019/1083). We make use of a biobank
474 (Unca-hT cell biobank) which was registered at FAGG (reference number at Bioresource center Ghent is
475 BR-109). The breeding of NSG mice is covered by file E-726 and animal experiments are covered by files
476 EC2020-009, EC2021-063 and EC2022-006.

477 Cell lines

478 We selected three tumor cell lines to study the anti-tumor functionality of the MGAT5 KO CD70 nanoCAR
479 T cells. THP-1 cells are a M4 subtype acute myeloid leukemia (AML) cell line[71], SKOV-3 cells are a highly
480 immunosuppressive human serous adenocarcinoma cell line[33,34,36,72] and Raji cells are a human B
481 lymphoblastoid cell line derived from a patient with Burkitt's lymphoma. We confirmed the cell surface
482 CD70 expression on these cells by flow cytometry (**Supplementary Figure 1**.A-B). Further, we confirmed

483 absence of CD70 expression on non-transduced (NTC) and CD70 nanoCAR transduced $CD3^+$ T cells. THP-1
484 cells were cultured in RPMI medium (Gibco) supplemented with 10% fetal calf serum (FCS), 0.03% L-Gln,
485 0.4 mM sodium pyruvate and 50 µM β-mercaptoethanol. SKOV-3 cells expressing luciferase were kindly
486 provided by Dr. Olivier De Wever[73] (Ghent University, Faculty of Medicine and Health Sciences) and were
487 cultured in DMEM medium (Gibco) supplemented with 10% FCS and 1% penicillin/streptomycin
488 (Pen/Strep). Jurkat cells were obtained from ATCC and were cultured in RPMI medium (Gibco)
489 supplemented with 10% FCS, 2mM L-Gln and 0.4 mM sodium pyruvate. Raji cells expressing luciferase were
490 generated at our labs and were cultured in RPMI medium (Gibco) supplemented with 10% FCS, 2mM L-
491 Gln, 0.4 mM sodium pyruvate, 50 µM β-mercaptoethanol and 1% Pen/Strep. All cell lines were maintained
492 in a 37°C, 5% CO_2, fully humidified incubator and passaged twice weekly. SKOV-3 cells are detached with
493 trypsin/EDTA and always seeded at 1 x 10^6 cells in a T175 falcon. Suspension cells were subcultured to
494 3.10^5 cells/mL (THP-1/Jurkat) or 5.10^5 cells/mL (Raji).

495 **Human $CD3^+$ T cell isolation and culturing**

496 Leukocyte-enriched buffy coat samples were obtained from healthy donors attending the Red Cross center
497 after informed consent and ethical committee approval. Peripheral blood lymphocytes were prepared by
498 Ficoll-Paque density centrifugation as described in the instruction manual for Leucosep™ (Greiner bio-
499 one). $CD3^+$ T cells were isolated by negative selection with antibodies against CD14, CD15, CD16, CD19,
500 CD36, CD56, CD123 and CD235 (MojoSort™ Human CD3 T cell selection kit, Biolegend) according to the
501 manufacturer's protocol. Cells were cultured in IMDM + Glutamax medium (Gibco-BRL) supplemented with
502 10% heat-inactivated FCS and stimulated with Immunocult™ Human CD3/CD28 T cell Activator (Stemcell
503 Technologies) (25 µL/ 10^6 cells) for 3 days at 37°C in the presence of 10 ng/ mL IL-12 (Biolegend).
504 Prior to cell seeding, cells were washed twice with PBS before putting them in culture with recombinant
505 human IL-7 at 10ng/mL (Miltenyi) and recombinant human IL-15 at 10 ng/mL (Miltenyi). Cytokines and
506 medium were replaced every 2-3 days. Cell densities were maintained between 1 x 10^6 and 3 x10^6 cells/
507 mL. In experiment with donors A, B, D, E, F, G, H, I, J and K, $CD3^+$ isolation was started from freshly prepared
508 PBMC cells while in the experiment with donor C, $CD3^+$ T cell isolation was started from a frozen batch of
509 PBMCs (Supplementary Table 3).

510 **Generating *MGAT5* KO nanoCAR T cells**

511 We first selected a CRISPR-Cas9 guide RNA (gRNA) to delete *MGAT5* in CAR T cells. We designed four gRNAs
512 using the Synthego design tool (https://www.synthego.com/products/bioinformatics/crispr-design-tool).
513 Guides were ordered as chemically modified synthetic sgRNAs (with 2'O-Methyl at three first and three
514 last bases and 3' phosphorothioate bonds between first three and last two bases) and reconstituted at 100
515 µM in TE buffer. After initial screening, we selected the most efficient sgRNA (**Supplementary Figure 2**) on
516 the basis of Sanger sequencing and evaluation of lectin staining as described below. We used this sgRNA

517 to knockout *MGAT5* in primary T cells using an optimized CAR T manufacturing process in which $CD3^+$ T
518 cells were stimulated with Immunocult for three days, after which activated T cells were first subjected to
519 Cas9 RNP nucleofection, followed by a retroviral transduction on the same day. Engineering efficiencies
520 were assessed on day 10. The experimental timeline is depicted in **Figure 1**.B.
521 Recombinant Cas9-GFP protein was purchased from the VIB protein core (https://vib.be/labs/vib-protein-
522 core). Cas9 RNP was made by incubating Cas9 protein with sgRNA at a molar ratio of 1:2 at 37°C for 15 min
523 immediately prior to electroporation in T cells. Electroporation was performed using the Lonza Amaxa 4D
524 Nucleofector X unit (Program EH-115) and the P3 primary cell kit with the following conditions: 1 x 10^6
525 cells/20 µL P3 buffer per cuvette (16-well strips) with 20 µM Cas9-RNP. Following nucleofection, 80 µL pre-
526 warmed medium was added per well and cells were allowed to rest for 30 mins at 37°C, 5% CO_2, before
527 they were collected in prewarmed medium, centrifuged for 5 min at 300 x g, counted and seeded on
528 retronectin-coated plates for transduction.
529 0.1 x 10^6 cells were collected and lysed in QuickExtract™ (Lucigen Epicentre) according to the supplier's
530 instructions. The target site was amplified by PCR (**Supplementary Figure 2**) and Sanger Sequenced.
531 Sequencing data was analyzed by variant deconvolution modelling with the ICE tool (Inference of CRISPR
532 Edits, Synthego) to infer the percentage of insertions and deletions (INDEL score) and the percentage of
533 insertions and deletions that are out of frame (KO score)[74]. Cutting and error-prone repair usually results
534 in mixed sequencing bases after the cut. %INDEL: % insertions/deletions, %KO: proportion of indels that
535 indicate a frameshift or are 21+ bp in length (assumes all edits are in a coding region), R2: model fit (how
536 well the proposed indel distribution fits the Sanger sequence data of the edited sample).

537 Production of retroviral vectors

538 In our work, we made use of a nanoCAR targeting CD70, an emerging target across several carcinomas and
539 B cell lymphoma, allowing to use the same nanoCAR design in xenograft models of both very different
540 tumor types. The nanobody used in this nanoCAR construct was identified previously at our center (Dr. Jan
541 Tavernier, VIB-UGent Center for Medical Biotechnology) and was built into standard 2nd-generation CAR
542 signaling domain architecture as described previously[26]. The retroviral construct encoding the nanoCAR
543 sequence was previously cloned in the LZRS-IRES-eGFP vector[26]. Viral particles were produced using
544 standard $Ca_3(PO_4)_2$ transfection of the Phoenix ampho packaging cell line[75]. Retroviral supernatant was
545 collected at day 14 after transfection and puromycin selection and kept at - 80°C until use.

546 Generation of CD70 nanoCAR Expressing Human T cells

547 Immunocult-stimulated human $CD3^+$ T cells were retrovirally transduced on Retronectin-coated plates
548 (TaKaRa). 500 µL of cells per well at 0.5 x 10^6 cells/mL were supplemented with 0.5 mL retroviral
549 supernatant and centrifuged for 90 minutes at 890 g at 32°C. Transduced cells were detected by eGFP
550 fluorescence or by staining with an anti-VHH antibody (iFluor555) directed against the nanobody

551 constituting the extracellular domain of the CAR and analyzed by flow cytometry. A minimum of 50 000
552 events was recorded.

553 **Lectin-based flow cytometry**

554 For the evaluation of the poly-LacNAc density on the cell surface, we used the lectin from *Datura*
555 *stramonium* and *Phaseolus Vulgaris* Leucoagglutinin (PHA-L), both at a staining concentration of 10 µg/ mL
556 (Vector laboratories, Biotinylated DSL: B-1185, Biotinylated PHA-L: B-1115). 2 x 10^5 cells per condition were
557 collected and rinsed three times with PBS. Cells were incubated with fixable viability dye eFl780
558 (eBioscience, 1000x dilution) and incubated for 30 minutes at 4°C in the dark. After washing the cells with
559 PBS, the cells were fixed with 4% paraformaldehyde (PFA), for 20 minutes at room temperature in the dark.
560 After rinsing with lectin binding buffer (LBB; PBS with 0.1 mM $CaCl_2$), cells were stained with biotinylated
561 lectin in LBB for 1 hour at 4°C. After this lectin staining, cells were washed in LBB before adding the PE-
562 coupled neutravidin (Invitrogen, 5 µg/mL) for 30 minutes at 4°C. After washing the cells with PBS, samples
563 were resuspended in LBB and analyzed by flow cytometry. A minimum of 50 000 events was recorded.

564 **PNGaseF digest and N-glycan analysis using CGE-LIF profiling**

565 In order to prepare cell surface N-glycans for CE-LIF profiling, 1 x 10^6 cells were collected per condition and
566 washed three times with PBS to reduce the presence of medium-derived glycans. Cell culture medium was
567 collected for N-glycan labeling. PNGaseF digest (0.125 IU/ 1x10^6 cells, in-house production) was performed
568 in 25 µL final volume in PBS for 2 hours at 37°C. Cells were removed by centrifugation (5 min at 300 x g)
569 and the supernatant was subjected to another centrifugation step (15 min at 15 000 rpm) to remove cell
570 debris. The remaining liquid portion of the sample was stored at -20°C until 8-aminopyrene-1,3,6-
571 trisulfonic acid (APTS) labeling and CE-LIF analysis.
572 The remaining N-glycan samples were labelled by adding an equal volume (20 µL) of labeling mix consisting
573 of a 1/1 v/v mix of 1M borane-morpholine complex in 20% DMSO, 20% SDS and 4M Urea mixed with 350
574 mM APTS in 2.4M citric acid and 14% SDS immediately prior to labeling. The labeling reaction was incubated
575 at 70°C for 1 hour and allowed to cool down at 4°C before purification. Size exclusion chromatography
576 (Sephadex G-10 resin with an exclusion limit of 700 Da prepared in a 96-well setup in Multiscreen-Durapore
577 plates) was performed twice to desalt the samples and to remove free unreacted APTS[76]. The labelled
578 glycans were then dried in a speedvac.
579 Purified labelled and dried N-glycans were resuspended in 10 µL of ultrapure water and analyzed with
580 capillary gel electrophoresis on an eight-capillary DNA sequencer (Applied Biosystems 3500 Genetic
581 analyzer). An internal standard (GlyXera) was added to the samples to be able to align profiles from
582 different samples. Samples were injected on a 50 cm capillary at 15 kV for 10 seconds, using POP7 polymer
583 and 100 mM TAPS, pH 8.0, containing 1 mM EDTA as the running buffer. N-glycan profiles were analyzed
584 through the Genemapper 6 software.

585 **Flow cytometry analysis**

586 Flow cytometry analysis was performed on 0.2 x 10^6 cells per sample collected in a 96-well U bottom plate.
587 Cells were rinsed with FACS buffer (PBS containing 0.5% BSA and 2mM EDTA) for 5 min at 300 x g and
588 incubated with Fc Receptor Blocking solution (Human TruStain FcX™, Biolegend) for 10 minutes prior to
589 cell surface staining with fluorescently labelled antibodies in Brilliant Stain buffer (BD Biosciences) for 30
590 minutes at 4°C.

591 For human $CD3^+$ T cell phenotyping, cells were labelled with fluorescent antibodies against human CD8,
592 CD62L and CD45RA (BD Biosciences) and CD3, CD4, CD25, CD69, and CD279 (PD-1) (Biolegend). A Fixable
593 dye eFluor™ 780 (eBioscience) was used to evaluate live/dead cells.

594 Flow cytometer calibration was performed using CS&T beads (BD Biosciences). The gating strategy was set
595 based on fluorescence minus one (FMO) controls and retained for all samples. Jurkat, THP-1, SKOV-3 and
596 Raji cell lines and primary human T cells were labelled with fluorescent antibody against human CD70
597 (PerCP-Cy5.5 labelled) or isotype control (Biolegend) to verify antigen expression as described before[77].

598 In all analyses, following doublet exclusion, live cells were identified using a fixable viability dye (Molecular
599 Probes, Life Technologies). Data were acquired on a BD Symphony A5 equipped with five lasers (355, 405,
600 488, 561, 640nm) (BD Biosciences) and analyzed using FlowJo software (Tree Star, Ashland, OR). Ultra-
601 rainbow fluorescent particles (Spherotech, Cat N° URFP-38-5A) are used for alignment in all channels
602 between different experiments. CountBright™ Absolute counting beads (Molecular Probes, Cat N°
603 11570066) were used to normalize cell counts. An overview of all flow cytometry antibodies used in this
604 study with details on fluorochrome, dilution, company and catalogue number are given in **Supplementary**
605 Table 4.

606 ***In vitro* analysis of cytokine production**

607 Glyco-engineered CD70 nanoCAR T cells were stimulated *in vitro* by co-incubation with THP-1 or SKOV-3
608 tumor cell lines expressing CD70 in a 96-well plate in duplicate. After 1 hour of co-incubation, BD GolgiPlug
609 (Fisher Scientific, 1:250) was added and after an additional 15 hours of stimulation, the cells were
610 harvested, labelled with fluorescent antibodies against CD3, CD4 and CD8, fixed and permeabilized
611 (Fixation/Permeabilization concentrate – diluent, eBioscience, Cat N° 00-513-43 and 00-5223-56) and
612 labelled for intracellular cytokine levels with fluorescent antibodies against TNF-α (BD Biosciences), IFN-γ
613 and IL-2 (Biolegend). Samples were analyzed by flow cytometry as described above.

614 ***In vitro*** **analysis of tumor cell killing**

615 Glyco-engineered CD70 nanoCAR T cells were incubated with 2 x 10^4 THP-1 cells at different effector/target
616 ratios (0; 0.0015; 0.015 and 0.15) in IMDM medium with Glutamax (Gibco) containing 10% FCS and 1%
617 Pen/Strep. Multiple runs of the same conditions were setup, allowing for flow cytometrical analysis at days
618 0, 3, 7, 10 and 14. In the wells remaining for analysis at day 10 and 14, 2 x 10^4 THP-1 cells were added at
619 day 7. Cells were labelled with fluorescent antibodies against CD3, CD4 and CD8 for the analysis of T cells
620 and CD33 for the detection of THP-1 cells.

621 **Statistical analysis of *in vitro* experiments**

622 To analyze the data of the fractions of cytokine-producing cells upon *MGAT5* glycoengineering (**Figure 1**.I-
623 J), we considered the control setup in which cells were not stimulated to represent a background signal.
624 We subtracted the mean percentage cytokine positive cells measured in the two technical repeats of non-
625 stimulated cells from the corresponding percentage of cytokine positive cells in the stimulated setups
626 (corresponding means of the setup with the same CAR engineering and donor). For each cytokine, we built
627 an ANOVA model in R[78], with Stimulation, Donor and Group as main effects (all coded as categorical) and
628 allowing for all two-way interactions. Model terms were tested via F tests. The effect of *MGAT5*
629 engineering, averaged over donors and stimulation strategies, was obtained from each final model using
630 the multcomp package[79] with sandwich estimators[80,81].

631 To analyze the number of mock Cas9 and MGAT5 KO CD70 nanoCAR cells in the THP-1 co-culture
632 experiments (**Figure 1**.L, M, N, O), we started from flow cytometry-based count data. Since the counts had
633 been normalized using counting beads, they were not necessarily integers so we rounded all to the closest
634 integer. We considered each setup with the same donor, E/T Ratio and type of CAR T cells (i.e. mock Cas9
635 CD70 nanoCAR or CD70 nanoCAR *MGAT5* KO) as a cluster. Since we had two measurements (technical
636 repeats) at each day and the measurements were performed at day 0, 4, 7, 11 and 14, this means we had
637 10 measurements in each cluster. Furthermore, we observed a slight rise in the counts of the NTC cells
638 over time in the control setups. We corrected the CAR T cell counts for this background (per cluster and at
639 each timepoint) by subtracting the mean background count from the measurements.

640 We analyzed the background-corrected counts with a generalized linear mixed model (GLMM) to allow for
641 modeling of the within-cluster correlation over time. Since the data showed considerable overdispersion,
642 the most appropriate choice was to use a negative binomial model (with a log link function). The
643 GLMMadaptive package[82] allows to fit such a model in R[78] using adaptive Gaussian quadrature (AGQ). We
644 did not have enough data to fit a random slope model, so we settled for a random intercept model of the
645 following model formula:

646 $$\text{Cell Count} \sim \text{Day}*(\text{Group} + \text{Donor} + \text{ETRatio}) + \text{Group}*\text{Donor} + (1|\text{cluster})$$

647 In this model, all predictors (Day, Group, Donor ETRatio) are coded as a categorical variable. We chose to
648 also model the time variable as categorical since the log-transformed counts do not evolve linearly with
649 time. Contrasts were estimated using the multcomp package[79].

650 *In vivo* analysis of glyco-engineered CD70 nanoCAR T cell tumor control efficacy in the SKOV-3 model

651 NSG mice (breeder pairs obtained from The Jackson Laboratory, breeding in house) between 8-12 weeks
652 of age were subcutaneously (in the right flank) injected with 2 x 10^6 luciferase-expressing SKOV-3 cells in
653 50 µL PBS. Ten days after tumor cell inoculation, after establishment of a solid, palpable tumor, mice were
654 treated with 3 x10^6 of either mock Cas9-engineered or MGAT5 KO CD70 nanoCAR (in 200 µL total volume
655 in PBS). As control groups, mice were treated with PBS to evaluate tumor development, or with non-
656 transduced T cells (NTC) to evaluate graft-versus-host disease (GvHD) and non-specific anti-tumor effects.
657 Body weight and tumor progression was followed up by caliper and BLI. A dose of 150 mg/kg D-luciferin
658 potassium salt (Perkin Elmer) was injected intraperitoneally 10 minutes before BLI. Imaging data were
659 analyzed using Living Image Software and reported as photons/second. Surviving mice were followed up
660 in time and challenged between day 87 and day 90 with a second tumor injection in the left flank (opposite
661 flank of first tumor injection) to mimic a tumor relapse, thus evaluating long-term anti-tumor control
662 efficacy. Again, tumor burden was evaluated over time and the mice were sacrificed between day 118 and
663 day 123 for endpoint analyses (see experimental timeline for details). For statistical analysis, the
664 'Untreated' group contains the data from all the mice that did not receive any CD70 nanoCAR T cells, and
665 thus includes untreated mice and mice treated with PBS or NTC (which all behaved similar with respect to
666 tumor control).

667 In the experiment with donor A, we started with 10 mice in the PBS and 6 mice in the NTC group and 12
668 mice in the CD70 nanoCAR mock Cas9/*MGAT5* KO groups. At day 34, 6 mice from the PBS group, 5 mice
669 from the NTC group, 5 mice from the CD70 nanoCAR mock Cas9 and 6 mice of the CD70 nanoCAR *MGAT5*
670 KO group were euthanized and used for analysis of CAR T cell numbers in the spleen and blood. The other
671 5 mice from the CD70 nanoCAR mock Cas9/*MGAT5* KO groups were kept for tumor rechallenge. In the
672 experiment with donor B, we started with 6 mice in the PBS and NTC group and 9 mice in the CD70 nanoCAR
673 mock Cas9/*MGAT5* KO groups. We also included 9 mice in a CD70 nanoCAR group (i.e. with cells that did
674 not receive mock nucleofection). All mice were kept for rechallenge, unless the pre-defined humane
675 endpoint was reached (which only occurred in control mice that did not receive CAR T treatment). Humane
676 endpoint is reached when mice lost > 20% of their body weight. In the experiment with donor C, we started
677 with 7 mice in the NTC group, 13 mice in the CD70 nanoCAR mock Cas9 group and 14 mice in the CD70
678 nanoCAR *MGAT5* KO group. All mice were kept for rechallenge, unless humane endpoint was reached
679 (occurring in non-CAR T treated control mice). At the start of each experiment, we also kept a group of 8

680 (donor A) or 10 (donor B/C) mice to be used as age-matched control (=PBS) group in the tumor rechallenge
681 phase of the experiment.

682 *In vivo* analysis of glyco-engineered nanoCAR T cell tumor control efficacies in the Raji model

683 Female NSG mice (breeder pairs obtained from The Jackson Laboratory, breeding in house) between 8-15
684 weeks of age were intravenously injected with 0.5 x 10^6 Raji cells in 50 µL of PBS. 4 x 10^6 CD70 nanoCAR T
685 cells were intravenously injected 7 days post-Raji injection (in 200 µL total volume in PBS). In preliminary
686 titration experiments using non-engineered CAR T cells from a different donor, we had determined that a
687 dose of 4 x 10^6 CD70 nanoCAR T cells per mouse yielded a delayed tumor growth in the intravenous Raji
688 model, while not being sufficient for survival, such that improvements in efficacy could be detectable by
689 increased survival rates. Body weight was followed up as was tumor progression by BLI. A dose of 150
690 mg/kg D-luciferin potassium salt (Perkin Elmer) was injected intraperitoneally 10 minutes before BLI.
691 Imaging data were analyzed using Living Image Software and reported as photons/second. In contrast to
692 the subcutaneous localized SKOV-3 carcinoma model, this Raji lymphoma model is one of hematogenous
693 aggressive metastasis, with tumors rapidly establishing in multiple organs, including the brain.
694 In the experiment with donor D, we started with 5 mice in all groups. In the experiment with donor E, we
695 started with 4 mice in all groups. In the experiment with donor F, we started with 5 mice in the NTC group,
696 5 mice in the mock Cas9 nanoCAR group and 4 mice in the MGAT5 KO CD70 nanoCAR groups. In the
697 experiment with donor G, we started with 7 mice in the NTC group, 8 mice in the mock Cas9 CD70 nanoCAR
698 group and 6 mice in the MGAT5 KO CD70 nanoCAR group.

699 Endpoint and intermediate analysis on spleen and blood

700 The presence and phenotype of CAR T cells was evaluated in the blood and spleen. Peripheral blood was
701 collected via the tail vein and transferred to EDTA coated Microvettes (Sarstedt) for intermediate analysis
702 at day 34 (donors A,B,C) and at days 80 (donor A), day 88 (donor B) and day 85 (donor C) in the SKOV-3
703 model and at day 27 (donor D, E and G), day 31 (donor F), day 95 (donor E), day 94 (donor F) and day 90
704 (donor G) in the Raji model. At the end of the experiments (see time lines for exact days on **Figure 2** and
705 **Figure 3**), blood was also collected after euthanasia and puncture of the right atrium of the heart. The
706 volume of blood was determined and red blood cells were removed using ammonium-chloride-potassium
707 (ACK) lysis buffer (added in a 1:20 blood:ACK volume ratio; Lonza) followed by neutralization in FACS buffer
708 and centrifugation at 300 x g for 5 min. Cells were counted prior to antibody staining for flow cytometry
709 analysis.
710 In the SKOV-3 model, spleens were dissected from all of the surviving mice at the end of the experiments,
711 (see time lines for exact days on **Figure 2**). For donor A, where all of the CAR T treated mice in both non-
712 engineered and MGAT5 KO groups had already cleared the tumor at day 34, half of the mice in the
713 experiment were euthanized at that timepoint for spleen investigation. Spleens were collected and

714 processed to a cell suspension through a 70 µM cell strainer. Cells were counted prior to antibody staining
715 for flow cytometry analysis.

716 **Statistical analyses *in vivo* experiments**

717 *FACS-based cell count data from blood and spleen (SKOV-3 model) with donors A, B and C and from blood*
718 *(Raji model) with donors E, F, G and H*

719 To compare the FACS-based cell-count data between the *MGAT5* KO and WT CAR T groups, we ran a
720 separate statistical model for each setting. For the SKOV-3 model, the settings are comprised of all unique
721 combinations of donor (A, B or C), timepoint (Early, Mid, Late/Endpoint), and tissue source (spleen).
722 Excluding settings for which data was lacking, this resulted in 13 statistical tests (see below) corresponding
723 to the panels in **Figure 2**.E and F. For the Raji model, the settings are comprised of all unique combinations
724 of donor (E, F, G, H), timepoint (timepoint 1, timepoint 2) and target (CD70). Excluding settings for which
725 data was lacking, this resulted in 13 statistical models (see below), corresponding to the panels in **Figure**
726 **3**.D. The lack of data for some settings of the blood count analysis should be read in the context of survival
727 curves presented in the same figure; in these groups, mice had already been euthanized or died at the time
728 of blood cell count analysis.

729 We ran quasi Poisson models in R[78], using the glm function with Cell Counts per mL of blood or number of
730 cells per spleen as the outcome variable and Group (*MGAT5* KO vs WT) as the predictor variable. The
731 presented p-values were then either directly extracted from the glm (Raji model), or calculated from the
732 glm using the multcomp package[79] (SKOV-3 model).

733 *Treatment of tumor-bearing mice with MGAT5 KO CD70 nanoCAR T cells leads to a better control of tumor*
734 *growth rate*

735 To evaluate differences in tumor growth or resolution between the treated mice, we fitted a generalized
736 linear mixed models (GLMMs). A separate model was fitted for data from each donor and the primary and
737 secondary tumor (**Supplementary Figure 4**, **Supplementary Figure 5**, **Supplementary Figure 6**). The main
738 reason for this is that the model would become unnecessarily complex because the timescales (design) of
739 both experiments differ slightly as do the times at which the mice start to respond to the CAR T cell therapy.
740 The latter is possibly due to inherent differences between the CAR T cell batches (i.e. a donor effect).

741 *Longitudinal analyses*

742 Tumor volumes were measured by measuring the length and width of a tumor and using the length*
743 width*width/2 (this is a half cube or cuboid) approximation of the volume of a sphere. We cross-checked
744 with BLI data for the small tumors, since this gives a better indication on whether there actually is still a
745 tumor present or whether the lesion is remnant scar tissue. Whenever a small tumor was measured or a
746 "zero volume" was registered (i.e. no morphological lesion remaining), BLI was used to verify whether
747 tumor cells were actually present or not and the caliper measurements were adapted accordingly: when

748 no tumor was found on BLI, we left the caliper measurements to zero, and when a tumor was found on BLI
749 but not measurable by caliper, we set the tumor volume equivalent to 0.0625 mm^3 (corresponding to 0.5
750 mm width/length).
751 We then analyzed the tumor volume data (in mm^3) of each experiment (donor A, B and C) and each phase
752 (primary tumor before and after rechallenge and secondary tumor) separately by fitting a GLMM to each
753 using the glmmTMB package[83] in R[78]. The models used a log link and a Tweedie error structure to
754 accommodate exact zeros and the mean-variance relationship in the data. Further, we used natural splines
755 (with df = 3 to 5) to model the (continuous) time variable in an interaction with the (categorical) group
756 variable. This allows for flexible modeling of the tumor volume in function of time in each treatment group.
757 Random effects included a per-mouse random intercept and, if necessary, a random slope for the time
758 variable to model within-mouse correlation over time. The models were fitted using REML. Contrasts were
759 calculated using the multcomp package[84] to obtain multiple-testing adjusted p-values and 95% confidence
760 intervals.
761 *Survival analysis (time to relapse)*
762 To analyze the time to relapse, we first defined the start of follow up as the moment the primary tumor
763 was controlled or partially controlled. We define control as the first day the tumor became completely
764 undetectable on BLI and by caliper measurement. We define partial control as the first day a tumor (that
765 never fully disappears) stopped increasing in size according to caliper measurements and no increase in
766 tumor volume was seen in at least 4 consecutive measurement days. Next, we define a relapse event as
767 the moment a tumor starts growing again. As the onset of relapse, we take the first day that the tumor
768 volume reaches again > 4 mm^3 and only when tumor growth is also seen in 4 consecutive measurement
769 days following that day. The time to event is then the time between start of follow up and a relapse event
770 and the follow up time is the time between start of follow up and either an event or the end of follow up
771 in case of no relapse. We used R[78] with the survival[85,86] and survminer[87] packages to generate Kaplan-Meier
772 plots with estimates of the median survival times and a corresponding risk and events table. Since relapses
773 were only observed in experiment with donor B, we ran a straightforward analysis with group as the only
774 predictor (groups: CD70 nanoCAR or CD70 nanoCAR - MGAT5 KO). We tested for the difference in survival
775 probability in these groups with a logrank test as implemented in the survival package.

776 ***Ex vivo* analysis of tumor cell killing**

777 SKOV-3 tumors in NSG mice were established, treated with CAR T cells and monitored as described above
778 (in this experiment with donor H and I). The number of mice treated were: non-transduced control (NTC)
779 (n=13), CD70 nanoCAR T (n=13), *MGAT5* KO CD70 nanoCAR T (n=9). Peripheral blood was collected via the
780 tail vein and transferred to EDTA coated Microvettes (Sarstedt). The volume of blood was determined and
781 red blood cells were removed using ACK lysis buffer (Lonza) prior to antibody staining for flow cytometry

782 analysis (determination of # circulating CAR T cells in the blood). Each sample was measured separately to
783 determine the amount of circulating CAR T cells. Afterwards, cells were pooled per condition. These blood
784 cells, containing differentially engineered CD70 nanoCAR T cells, were incubated with 2 x 10^4 THP-1 cells
785 at different effector/target ratios (i.e. cells isolated from 50µL of blood and from 40µL of blood) in IMDM
786 medium with Glutamax (Gibco) containing 10% FCS and 1% Pen/Strep. Cells were labelled with fluorescent
787 antibodies against CD3, CD4 and CD8 for the analysis of T cells and CD33 for the detection of THP-1 cells,
788 at the start of the co-culture (day 0) and at day 4, 8, 11 and 14. At day 8 of co-culture, 2 x 10^4 THP-1 cells
789 were added to the remaining wells for analysis at day 11 and 14. Cell numbers were determined by flow
790 cytometry.

791 CD107a degranulation assay

792 Membrane expression of CD107a represents a surrogate marker of cytotoxicity of activated and
793 degranulating immune cells. Recombinant Human CD27 Ligand (R&D systems) was coated overnight at
794 different concentrations (0.01 – 10 µg/mL) on the surface of a 96-well plate (Falcon™ clear flat bottom TC,
795 Corning, France) at 4°C. Before the addition of the cells/anti-CD107a antibody, the recombinant human
796 CD27 ligand was removed from the plates and the wells were washed 1x with PBS. CAR T cells (from donor
797 K) were put at 1 x 10^6 cells/mL (corrected based on %GFP-positivity) and mixed with anti-CD107a-BUV395
798 antibody at a 10:1 ratio. 50µL of this mix was added per well of the coated 96-well plate. In the control
799 condition, 1,25µL of Immunocult™ Human CD3/CD28 T cell Activator was added (25 µL/ 10^6 cells). Plates
800 were incubated for 1 hour at 37°C C and 5% CO_2, and for an additional 4 h in the presence of the secretion
801 inhibitor Brefeldin A (Cayman Chemical).
802 We analyzed the results for CD107a staining on CAR T cells with anti-CD107a-BUV395 (BD Biosciences) and
803 anti-CD3-BV510 (Miltenyi Biotec) antibodies, in combination with eFluor780 viability dye (Ebioscience) on
804 GFP-positive cells using flow cytometry (BD Symphony A5).

805 Cytokine Independent growth assay

806 Human $CD3^+$ T cells were isolated and engineered as described (from donor G). Ten days after engineering
807 and cultivation with IL-7/IL-15, engineered CAR T cells were cultured in IMDM + Glutamax medium (Gibco-
808 BRL) supplemented with 10% heat-inactivated FCS with or without supplemental cytokines. All cells were
809 maintained at a cell density of <1.0 x 10^6 cells/mL over the course of the experiment. Total cell counts of
810 cells cultured in IMDM with or without supplemental cytokines was monitored for 14 days. Cells cultured
811 in IMDM with supplemental cytokines were given 10 ng/mL of IL-7 and IL-15 on day 0 and subsequently
812 maintained with IMDM containing IL-7 and IL-15 until day 14.

813 Single cell RNA sequencing (scRNAseq)

814 *Preparation cells from tumor*

815 SKOV-3 tumor inoculation and CD70 nanoCAR T treatment was performed as described above. Cells from
816 donor J were used. Tumors were collected in PBS and transferred into a gentleMACS C tube (Miltenyi)
817 containing digestion buffer (MEMα (Capricorn), 1% Pen/strep (Sigma), 50 µM β-mercaptoethanol (Gibco),
818 0,1 mg/mL DNAse I (Roche), 0.125 mg/mL Collagenase D (Roche), 0,1 mg/mL dispase II (Sigma)),
819 GentleMACS C tubes are loaded in the MACS dissociator without heaters and progam h_cord1 was run.
820 The tubes were subsequently incubated at 37°C for 40 min, and vortexed every 10 minutes. After that, the
821 tubes were put on ice and 10mL of ice cold FACS buffer is added to the tube, before passing the suspension
822 through a 70µm cell strainer. The strainer is washed with 10mL FACS buffer and cells are pelleted at 300 x
823 g, 5 min at 4°C. Cells are resuspended in FACS buffer before proceeding with staining.

824 *Single cell library preparation and sequencing*

825 Mice were sacrificed seven days post nanoCAR T cell injection (from donor J). Peripheral blood was taken
826 following severing of the right atrium of the heart and transferred to EDTA coated Microvettes (Sarstedt).
827 The volume of blood was determined and red blood cells were removed using ACK lysis buffer (Lonza) prior
828 to antibody staining. Tumors were isolated and processed to obtain a single cell suspension as described
829 above. Single cell suspensions from 6 mice/condition were pooled and labelled with anti-human CD45-
830 PerCP-Cy5.5 antibody (BD Biosciences) and a unique human TotalSeq-C hashing antibody (Biolegend)
831 diluted 1:250. To enable multiplexing, we applied a cellular hashing strategy using TotalSeq-C anti-human
832 hashtag antibodies specific against human CD298 and B2M (BioLegend). Each sample received a distinct
833 TotalSeq-C barcode, allowing downstream demultiplexing and assignment of single-cell transcriptomic
834 data to individual samples/conditions. FACS-sorted $CD45^+$ single-cell suspensions were resuspended at an
835 estimated final concentration of 1000 cells/µL, and loaded on a Chromium GemCode Single Cell Instrument
836 (10× Genomics) to generate single-cell Gel beads-in-EMulsion (NextGEM). The cDNA libraries were
837 prepared using the GemCode Single Cell 5′ v3 Gel Bead and Library kit, version 5.2 according to the
838 manufacturer's instructions (10x Genomics). Size selection with SPRIselect Reagent Kit (Beckman Coulter,
839 B23318) was used to separate amplified cDNA molecules for 5′ gene expression and cell surface protein
840 construction libraries. The cDNA content of pre-fragmentation and post-sample index PCR samples was
841 analyzed using the Fragment Analyzer (Agilent). Sequencing libraries were loaded on an Illumina NovaSeq
842 flow cell at VIB Nucleomics core on the Illumina NovaSeq 6000 platform with a read configuration of 28
843 cycles for Read 1 (which reads the 16bp 10x GEM-cell barcode followed by the 10bp UMI), 10 cycles for i7
844 index (which reads one of the sample barcodes), 10 cycles for i5 index (which is used for dual indexing),
845 and 90 cycles for Read 2 (which reads the cDNA and de feature barcode (TotalSeq/antibody tags). 1% PhiX

846 DNA was incorporated as a sequencing control, pooled in a 90:10 ratio for the combined 5′ gene expression
847 and cell surface protein samples, respectively.

848 *Processing of scRNA-seq and hashtag data*

849 The Cell Ranger pipeline (10× Genomics, version 7.2.0) was used to perform sample demultiplexing and to
850 generate FASTQ files for read 1, read 2, and the i5, i7 sample index for the gene expression protein libraries.
851 Read 2 of the gene expression libraries was mapped to the reference genome GRCh38. Subsequent
852 barcode processing, unique molecular identifiers, filtering, and gene counting was performed using the
853 Cell Ranger suite (10× Genomics). Downstream analyses were performed with Seurat[88] (version 5.0.0). In
854 order to maintain explicit control over all gene and cell quality control filters, we used the raw feature-
855 barcode matrix generated by CellRanger. Raw counts of the samples were normalized using global-scaling
856 normalization and log-transform method using the Seurat NormalizeData function with default
857 parameters. Feature counts for each cell are divided by the total counts for that cell and multiplied by the
858 scale.factor = 10,000 followed by natural-log transformation using log1p. Initial dimensionality reduction
859 and clustering was performed using the Seurat functions FindVariableFeatures, RunPCA, FindNeighbors
860 and FindClusters, with default parameters. Hashtag demultiplexing was performed using Seurat's
861 HTODemux and MultiSeq and we required agreement of both algorithms for the assignment of cells to
862 their respective biological samples. Cells with inconsistent demultiplexing calls, as well as cells identified as
863 negative and double were removed. Next, we excluded all cells with detection of transcripts of less than
864 200 genes, as well as genes expressed in less than 3 cells. Subsequently, clusters of mouse cells were
865 identified and removed based on overrepresentation of reads mapping to the mouse genome. After
866 excluding incorrectly demultiplexed cells and mouse cells, we obtained data on 12039 cells across four
867 samples under analysis (mock engineered versus MGAT5 KO CD70 nanoCAR T cells, circulating in blood vs
868 tumor-infiltrating). We repeated dimensionality reduction and clustering on the Seurat functions
869 FindVariableFeatures, RunPCA, FindNeighbors and FindClusters, using the 2000 most variable genes, 12
870 first principal components and cluster resolution of 0.5. Unsupervised Uniform Manifold Approximation
871 and Projection (UMAP) analyses implemented in the Seurat pipeline were further used to identify the major
872 cell populations. Tumor-infiltrating CAR T cells clustered separately from circulating CAR T cells. For
873 improved discrimination of CD4 and CD8 cells, clustering was further refined using the FindSubCluster
874 function using resolution up to 0.2 and manual curation. CellCycleScoring function was used to distinguish
875 cells in different cell cycle phases. Finally, cell clusters were labelled based on their association with
876 biological samples, CD4 and CD8 expression and proliferation state. Differential gene expression analysis
877 between conditions within the same cell cluster was performed using FindMarkers function with Wilcoxon
878 Rank Sum test for genes expressed in at least 25% cells of one of the compared populations and minimal
879 fold change threshold of 0.1, using the Bonferroni-corrected p-value of at least 0.05. Gene identifier

880 conversions were performed using biomaRt version 2.58.2 and human Ensembl database version 113 (Oct
881 2024). Comparison to custom gene sets of differentially expressed proteins from other studies was
882 performed using the gene set enrichment function of the clusterProfiler package[89] (version 4.10.1).
883 Enrichment analyses of pathways from KEGG, WikiPathways and Reactome databases were performed
884 using packages clusterProfiler (version 4.10.1), ReactomePA[90] (version 1.46.0) and enrichR[91] (version 3.2)
885 with Benjamini-Hochberg adjusted p-value cutoff of 0.1. Reactome pathways were further narrowed down
886 based on the presence of significant DE genes and average gene log2FC. Shared genes were additionally
887 used to remove redundancy between pathways. Full results are available is **Supplementary Table 2**

888 **Amnis ImagestreamX Mark II data acquisition**

889 Samples were analyzed on a Cytek® Amnis® ImagestreamX MkII imaging flow cytometer using Cytek Amnis
890 INSPIRE software version 6.2 (Merck Millipore, Nottingham UK). Prior to experimental analysis, following
891 the manufacturer's instructions for appropriate ImageStream X Mark II® set up and quality control
892 procedures, system calibrations were performed using ImageStream X Mark II® SpeedBead calibration
893 reagents. 100 µL aliquots of cell suspensions (SKOV-3, THP-1, Raji) at a concentration of $\sim 2\times10^7$ cells/mL in
894 PBS were prepared in 1.5 mL Eppendorfs. Prior to data collection, laser intensities were balanced to limit
895 saturation events and fluorescence channel overspill. For data acquisition an INSPIRE® template was set
896 up for in-focus and single cellular event gating, using Aspect Ratio and Root Mean Square (RMS) features,
897 ensuring collected cells were sufficiently circular and in focus. Data were acquired at a low velocity of 66.0
898 mm/s, with single cell events being collected at a magnification of×40. Acquisition of the images for CD70-
899 PerCP-Cy5-5 and Live/Dead eFl780 fluorescence assessment occurred in Channel 5 and 12; bright field:
900 channel 1 and 9; Side scatter: Channel 6. Data analysis was performed using IDEAS® software version 6.0.
901 For SKOV-3 cells 6519 single cells were analyzed, for THP-1 cells: 6208 single cells; for Raji cells: 4830 single
902 cells. Area (μm^2) and antigen staining intensity for each single event was determined and averages per cell
903 were calculated. Intensity/μm^2 was plotted.

904 **Data availability**

905 The single cell RNA sequencing data that support the findings of this study are openly available in the Gene
906 Expression Omnibus (GEO) (GSE301470). Code for the statistical analysis and visualization is made available
907 at GitHub (https://github.com/CallewaertLab/MGAT5KO_CART_manuscript).

908

909 ## Acknowledgements

910 Research of EDB was funded through a predoctoral fellowship at FWO, a doctor-assistant mandate at
911 UGent and an IOF Advanced project – F2024/IOF – Advanced/031. MG and LDP were funded through a
912 predoctoral fellowship of FWO. SDM is a junior post-doctoral fellow at FWO supported by the personal

913 grant 12AP724N. This work was further supported by grants G050420N and G028220N of FWO
914 Vlaanderen, a Young Investigator Proof of Concept (YIPOC) grant of the Cancer Research Institute Ghent
915 (CRIG), a Stichting tegen Kanker grant (F/2022/2010) and by the European Union (ERC Advanced Grant,
916 GlycoCAR, Horizon 101098331) as well as by institutional core funding of VIB. We thank Prof. Dr. Y. Chen
917 (Parker Institute for Cancer Immunotherapy Center at UCLA, Los Angeles, CA, USA) for intensive
918 experimental training in the CAR T field and Prof. J. Tavernier for providing the anti-CD70 nanobody used
919 in our CAR designs. We thank the VIB Bioimaging core Ghent (https://vib.be/labs/vib-bioimaging-core-
920 ghent), the VIB Flow Core Ghent (https://vib.be/labs/vib-flow-core-ghent), the VIB Nucleomics Core
921 (https://nucleomicscore.sites.vib.be/en) and the VIB Single Cell core (https://singlecellcore.sites.vib.be/en)
922 for technical support and infrastructure access. We thank Prof. O. De Wever (Ghent University, Faculty of
923 Medicine and Health Sciences) for providing the SKOV-3 cells expressing luciferase. N.C. dedicates this
924 study to the memory of his father Eric Callewaert, who succumbed in the course of our work to one of the
925 tumor types studied here.

926 Declaration of interest statement

927 EDB, NF and NC are co-inventors on an International Patent application (WO/2023/111322) by VIB and
928 Ghent University, which incorporates inventions described here. None of the other authors declares a
929 conflict of interest.

930 References

931 1. De Bousser E, Callewaert N, Festjens N. T Cell Engaging Immunotherapies, Highlighting Chimeric
932 Antigen Receptor (CAR) T Cell Therapy. Cancers 2021; 13:6067.

933 2. Vairy S, Garcia JL, Teira P, Bittencourt H. CTL019 (tisagenlecleucel): CAR-T therapy for relapsed and
934 refractory B-cell acute lymphoblastic leukemia. Drug Des Devel Ther 2018; 12:3885–98.

935 3. Reagan PM, Friedberg JW. Axicabtagene ciloleucel and brexucabtagene autoleucel in relapsed and
936 refractory diffuse large B-cell and mantle cell lymphomas. Future Oncol Lond Engl 2021; 17:1269–83.

937 4. Liu L, Qu Y, Cheng L, Yoon CW, He P, Monther A, Guo T, Chittle S, Wang Y. Engineering chimeric antigen
938 receptor T cells for solid tumour therapy. Clin Transl Med 2022; 12:e1141.

939 5. Uslu U, June CH. Beyond the blood: expanding CAR T cell therapy to solid tumors. Nat Biotechnol 2024;
940 :1–10.

941 6. Okada M, Chikuma S, Kondo T, Hibino S, Machiyama H, Yokosuka T, Nakano M, Yoshimura A. Blockage
942 of Core Fucosylation Reduces Cell-Surface Expression of PD-1 and Promotes Anti-tumor Immune
943 Responses of T Cells. Cell Rep 2017; 20:1017–28.

944 7. Lau KS, Partridge EA, Grigorian A, Silvescu CI, Reinhold VN, Demetriou M, Dennis JW. Complex N-Glycan
945 Number and Degree of Branching Cooperate to Regulate Cell Proliferation and Differentiation. Cell
946 2007; 129:123–34.

947 8. Kuball J, Hauptrock B, Malina V, Antunes E, Voss R-H, Wolfl M, Strong R, Theobald M, Greenberg PD.
948 Increasing functional avidity of TCR-redirected T cells by removing defined N-glycosylation sites in the
949 TCR constant domain. J Exp Med 2009; 206:463–75.

950 9. Demotte N, Wieërs G, Van Der Smissen P, Moser M, Schmidt C, Thielemans K, Squifflet J-L, Weynand
951 B, Carrasco J, Lurquin C, et al. A galectin-3 ligand corrects the impaired function of human CD4 and
952 CD8 tumor-infiltrating lymphocytes and favors tumor rejection in mice. Cancer Res 2010; 70:7476–88.

953 10. Demotte N, Stroobant V, Courtoy PJ, Van Der Smissen P, Colau D, Luescher IF, Hivroz C, Nicaise J,
954 Squifflet JL, Mourad M, et al. Restoring the Association of the T Cell Receptor with CD8 Reverses Anergy
955 in Human Tumor-Infiltrating Lymphocytes. Immunity 2008; 28:414–24.

956 11. Laderach DJ, Compagno D. Inhibition of galectins in cancer: Biological challenges for their clinical
957 application. Front Immunol 2023, 13:1104625.

958 12. Wang H, Kaur G, Sankin AI, Chen F, Guan F, Zang X. Immune checkpoint blockade and CAR-T cell
959 therapy in hematologic malignancies. J Hematol OncolJ Hematol Oncol 2019; 12:59.

960 13. Lv Y, Ma X, Ma Y, Du Y, Feng J. A new emerging target in cancer immunotherapy: Galectin-9 (LGALS9).
961 Genes Dis 2023; 10:2366–82.

962 14. Cabral J, Hanley SA, Gerlach JQ, O'Leary N, Cunningham S, Ritter T, Ceredig R, Joshi L, Griffin MD.
963 Distinctive Surface Glycosylation Patterns Associated With Mouse and Human $CD4^+$ Regulatory T Cells
964 and Their Suppressive Function. Front Immunol 2017; 8:987.

965 15. Earl LA, Bi S, Baum LG. N- and O-Glycans Modulate Galectin-1 Binding, CD45 Signaling, and T Cell Death.
966 J Biol Chem 2010; 285:2232–44.

967 16. Demetriou M, Granovsky M, Quaggin S, Dennis JW. Negative regulation of T-cell activation and
968 autoimmunity by Mgat5 N -glycosylation. Nature 2001; 409:733.

969 17. Togayachi A, Kozono Y, Ishida H, Abe S, Suzuki N, Tsunoda Y, Hagiwara K, Kuno A, Ohkura T, Sato N, et
970 al. Polylactosamine on glycoproteins influences basal levels of lymphocyte and macrophage activation.
971 Proc Natl Acad Sci U S A 2007; 104:15829–34.

972 18. Ye L, Park JJ, Dong MB, Yang Q, Chow RD, Peng L, Du Y, Guo J, Dai X, Wang G, et al. In vivo CRISPR
973 screening in CD8 T cells with AAV– Sleeping Beauty hybrid vectors identifies membrane targets for
974 improving immunotherapy for glioblastoma. Nat Biotechnol 2019; 37:1302–13.

975 19. Alegre ML, Frauwirth KA, Thompson CB. T-cell regulation by CD28 and CTLA-4. Nat Rev Immunol 2001;
976 1:220–8.

977 20. Morgan R, Gao G, Pawling J, Dennis JW, Demetriou M, Li B. N-acetylglucosaminyltransferase V (Mgat5)-
978 mediated N-glycosylation negatively regulates Th1 cytokine production by T cells. J Immunol Baltim
979 Md 1950 2004; 173:7200–8.

980 21. Smith LK, Boukhaled GM, Condotta SA, Mazouz S, Guthmiller JJ, Vijay R, Butler NS, Bruneau J, Shoukry
981 NH, Krawczyk CM, et al. Interleukin-10 Directly Inhibits CD8+ T Cell Function by Enhancing N-Glycan
982 Branching to Decrease Antigen Sensitivity. Immunity 2018; 48:299-312.e5.

983 22. Cedeno-Laurent F, Opperman M, Barthel SR, Hays D, Schatton T, Zhan Q, He X, Matta KL, Supko JG,
984 Frank MH, et al. Metabolic inhibition of galectin-1-binding carbohydrates accentuates anti-tumor
985 immunity. J Invest Dermatol 2012; 132:410–20.

986 23. Demotte N, Stroobant V, Courtoy PJ, Van Der Smissen P, Colau D, Luescher IF, Hivroz C, Nicaise J,
987 Squifflet J-L, Mourad M, et al. Restoring the Association of the T Cell Receptor with CD8 Reverses
988 Anergy in Human Tumor-Infiltrating Lymphocytes. Immunity 2008; 28:414–24.

989 24. Gagneux P, Panin V, Hennet T, Aebi M, Varki A. Evolution of Glycan Diversity [Internet]. In: Varki A,
990 Cummings RD, Esko JD, Stanley P, Hart GW, Aebi M, Mohnen D, Kinoshita T, Packer NH, Prestegard JH,
991 et al., editors. Essentials of Glycobiology. Cold Spring Harbor (NY): Cold Spring Harbor Laboratory Press;
992 2022; glycobiology.4e.20.

993 25. Ayala Ceja M, Khericha M, Harris CM, Puig-Saus C, Chen YY. CAR-T cell manufacturing: Major process
994 parameters and next-generation strategies. J Exp Med 2024; 221:e20230903.

995 26. De Munter S, Buhl JL, De Cock L, Van Parys A, Daneels W, Pascal E, Deseins L, Ingels J, Goetgeluk G,
996 Jansen H, et al. Knocking Out CD70 Rescues CD70-Specific NanoCAR T Cells from Antigen-Induced
997 Exhaustion. Cancer Immunol Res 2024; 12:1236–51.

998 27. Laroy W, Contreras R. Glycoprofiling by DNA Sequencer-Aided Fluorophore-Assisted Carbohydrate
999 Electrophoresis. In: Appasani K, Southern EM, editors. Bioarrays: From Basics to Diagnostics. Totowa,
1000 NJ: Humana Press; 2007; page 191–200.

1001 28. Vanderschaeghe D, Szekrényes Á, Wenz C, Gassmann M, Naik N, Bynum M, Yin H, Delanghe J, Guttman
1002 A, Callewaert N. High-Throughput Profiling of the Serum N-Glycome on Capillary Electrophoresis
1003 Microfluidics Systems: Toward Clinical Implementation of GlycoHepatoTest. Anal Chem 2010;
1004 82:7408–15.

1005 29. Meehl M, Ibanez J, Ward MB, Krenciute G. 295 Investigating the biological drivers of effective CAR T
1006 cell donors. J Immunother Cancer 2024;12(Suppl 2):A1–A1683.

1007 30. Lee W, Rose D, Keck JG, Yang J. Abstract 3850: Modeling individual variability in CD19 CAR-T therapy:
1008 An in vivo study with PBMC-humanized mice. Cancer Res 2024; 84:3850.

1009 31. Ayala Ceja M, Khericha M, Harris CM, Puig-Saus C, Chen YY. CAR-T cell manufacturing: Major process
1010 parameters and next-generation strategies. J Exp Med 2024; 221:e20230903.

1011 32. Maletzki C, Bock S, Fruh P, Macius K, Witt A, Prall F, Linnebacher M. NSG mice as hosts for oncological
1012 precision medicine. Lab Invest 2019; :1–11.

1013 33. Liu C, Zhang L, Chang X, Cheng Y, Cheng H, Ye X, Fu T, Chen J, Cui H. Overexpression and
1014 Immunosuppressive Functions of Transforming Growth Factor 1, Vascular Endothelial Growth Factor
1015 and Interleukin-10 in Epithelial Ovarian Cancer. Chin J Cancer Res 2012; 24:130–7.

1016 34. Li X, Ye F, Chen H, Lu W, Wan X, Xie X. Human ovarian carcinoma cells generate CD4+CD25+ regulatory
1017 T cells from peripheral CD4+CD25− T cells through secreting TGF-β. Cancer Lett 2007; 253:144–53.

1018 35. Shang W, Xu R, Xu T, Wu M, Xu J, Wang F. Ovarian Cancer Cells Promote Glycolysis Metabolism and
1019 TLR8-Mediated Metabolic Control of Human CD4+ T Cells. Front Oncol 2020; 10:570899.

1020 36. Liu H, Zhang G, Huang J, Ma S, Mi K, Cheng J, Zhu Y, Zha X, Huang W. Atractylenolide I modulates
1021 ovarian cancer cell-mediated immunosuppression by blocking MD-2/TLR4 complex-mediated
1022 MyD88/NF-κB signaling in vitro. J Transl Med 2016; 14:104.

1023 37. Chao MP, Alizadeh AA, Tang C, Myklebust JH, Varghese B, Gill S, Jan M, Cha AC, Chan CK, Tan BT, et al.
1024 Anti-CD47 antibody synergizes with rituximab to promote phagocytosis and eradicate non-Hodgkin
1025 lymphoma. Cell 2010; 142:699–713.

1026 38. Deng W, Chen P, Lei W, Xu Y, Xu N, Pu JJ, Liang A, Qian W. CD70-targeting CAR-T cells have potential
1027 activity against CD19-negative B-cell Lymphoma. Cancer Commun 2021; 41:925–9.

1028 39. Iyer SP, Sica RA, Ho PJ, Prica A, Zain J, Foss FM, Hu B, Beitinjaneh A, Weng W-K, Kim YH, et al. Safety
1029 and activity of CTX130, a CD70-targeted allogeneic CRISPR-Cas9-engineered CAR T-cell therapy, in
1030 patients with relapsed or refractory T-cell malignancies (COBALT-LYM): a single-arm, open-label, phase
1031 1, dose-escalation study. Lancet Oncol 2025; 26:110–22.

1032 40. Milacic M, Beavers D, Conley P, Gong C, Gillespie M, Griss J, Haw R, Jassal B, Matthews L, May B, et al.
1033 The Reactome Pathway Knowledgebase 2024. Nucleic Acids Res 2024; 52:D672–8.

1034 41. Ricciardi S, Manfrini N, Alfieri R, Calamita P, Crosti MC, Gallo S, Müller R, Pagani M, Abrignani S, Biffo
1035 S. The Translational Machinery of Human CD4+ T Cells Is Poised for Activation and Controls the Switch
1036 from Quiescence to Metabolic Remodeling. Cell Metab 2018; 28:895-906.e5.

1037 42. Good CR, Aznar MA, Kuramitsu S, Samareh P, Agarwal S, Donahue G, Ishiyama K, Wellhausen N,
1038 Rennels AK, Ma Y, et al. An NK-like CAR T cell transition in CAR T cell dysfunction. Cell 2021; 184:6081-
1039 6100.e26.

1040 43. Umaña P, Jean-Mairet J, Moudry R, Amstutz H, Bailey JE. Engineered glycoforms of an
1041 antineuroblastoma IgG1 with optimized antibody-dependent cellular cytotoxic activity. Nat Biotechnol
1042 1999; 17:176–80.

1043 44. Kanda Y, Yamada T, Mori K, Okazaki A, Inoue M, Kitajima-Miyama K, Kuni-Kamochi R, Nakano R, Yano
1044 K, Kakita S, et al. Comparison of biological activity among nonfucosylated therapeutic IgG1 antibodies
1045 with three different N-linked Fc oligosaccharides: the high-mannose, hybrid, and complex types.
1046 Glycobiology 2007; 17:104–18.

1047 45. Yamane-Ohnuki N, Kinoshita S, Inoue-Urakubo M, Kusunoki M, Iida S, Nakano R, Wakitani M, Niwa R,
1048 Sakurada M, Uchida K, et al. Establishment of FUT8 knockout Chinese hamster ovary cells: An ideal
1049 host cell line for producing completely defucosylated antibodies with enhanced antibody-dependent
1050 cellular cytotoxicity. Biotechnol Bioeng 2004; 87:614–22.

1051 46. Mizushima T, Yagi H, Takemoto E, Shibata-Koyama M, Isoda Y, Iida S, Masuda K, Satoh M, Kato K.
1052 Structural basis for improved efficacy of therapeutic antibodies on defucosylation of their Fc glycans.
1053 Genes Cells Devoted Mol Cell Mech 2011; 16:1071–80.

1054 47. Ferrara C, Brünker P, Suter T, Moser S, Püntener U, Umaña P. Modulation of therapeutic antibody
1055 effector functions by glycosylation engineering: influence of Golgi enzyme localization domain and co-
1056 expression of heterologous beta1, 4-N-acetylglucosaminyltransferase III and Golgi alpha-mannosidase
1057 II. Biotechnol Bioeng 2006; 93:851–61.

1058 48. Dalle S, Reslan L, Besseyre de Horts T, Herveau S, Herting F, Plesa A, Friess T, Umana P, Klein C,
1059 Dumontet C. Preclinical studies on the mechanism of action and the anti-lymphoma activity of the
1060 novel anti-CD20 antibody GA101. Mol Cancer Ther 2011; 10:178–85.

1061 49. Beck A, Reichert JM. Marketing approval of mogamulizumab. mAbs 2012; 4:419–25.

1062 50. Lee AJ, Ashkar AA. The Dual Nature of Type I and Type II Interferons. Front Immunol 2018; 9:2061.

1063 51. Badr HA, AlSadek DMM, El-Houseini ME, Saeui CT, Mathew MP, Yarema KJ, Ahmed H. Harnessing
1064 cancer cell metabolism for theranostic applications using metabolic glycoengineering of sialic acid in
1065 breast cancer as a pioneering example. Biomaterials 2017; 11:044.

1066 52. Wang H, Engesser J, Khatri R, Schaub DP, Paust H-J, Sultana Z, Jauch-Speer S-L, Peters A, Kaffke A, Bonn
1067 S, et al. Type I interferon drives T cell cytotoxicity by upregulation of interferon regulatory factor 7 in
1068 autoimmune kidney diseases in mice. Nat Commun 2025; 16:4686.

1069 53. Sumida TS, Dulberg S, Schupp JC, Lincoln MR, Stillwell HA, Axisa P-P, Comi M, Unterman A, Kaminski N,
1070 Madi A, et al. Type I interferon transcriptional network regulates expression of coinhibitory receptors
1071 in human T cells. Nat Immunol 2022; 23:632–42.

1072 54. Mihaescu G, Chifiriuc MC, Filip R, Bleotu C, Ditu LM, Constantin M, Cristian R-E, Grigore R, Bertesteanu
1073 SV, Bertesteanu G, et al. Role of interferons in the antiviral battle: from virus-host crosstalk to
1074 prophylactic and therapeutic potential in SARS-CoV-2 infection. Front Immunol 2024; 14:1273604.

1075 55. Qin Z, Xu T. Deciphering the deterministic role of TCR signaling in T cell fate determination. Front
1076 Immunol 2025; 16.

1077 56. Cao X, Liang Y, Hu Z, Li H, Yang J, Hsu EJ, Zhu J, Zhou J, Fu Y-X. Next generation of tumor-activating type
1078 I IFN enhances anti-tumor immune responses to overcome therapy resistance. Nat Commun 2021;
1079 12:5866.

1080 57. Harrer DC, Schenkel C, Bezler V, Kaljanac M, Hartley J, Barden M, Pan H, Holzinger A, Herr W, Abken
1081 H. CAR Triggered Release of Type-1 Interferon Limits CAR T-Cell Activities by an Artificial Negative
1082 Autocrine Loop. Cells 2022; 11:3839.

1083 58. Jung I-Y, Bartoszek RL, Rech AJ, Collins SM, Ooi S-K, Williams EF, Hopkins CR, Narayan V, Haas NB, Frey
1084 NV, et al. Type I Interferon Signaling via the EGR2 Transcriptional Regulator Potentiates CAR T Cell-
1085 Intrinsic Dysfunction. Cancer Discov 2023; 13:1636–55.

1086 59. Huang M, Zhao L, Cheng Y, Huang L, Zhou J, Li D, Wang J, Cao Y. Type I Interferon Impairs the Function
1087 of CAR-T Cells By Disrupting Immune Synapse Assembly. Blood 2024; 144:3407.

1088 60. Tang E, Hu Y, Cao G, Asby NW, Nguyen D-T, Aboelella NS, Ruiz H, Zhao Y, Xie L, Chen X, et al. Low-
1089 Strength Type I Interferon Signaling Promotes CAR T-Cell Treatment Efficacy. 2025; Available from:
1090 https://www.biorxiv.org/content/10.1101/2025.05.13.653878v1

1091 61. Moradi V, Khodabandehloo E, Alidadi M, Omidkhoda A, Ahmadbeigi N. Progress and pitfalls of gene
1092 editing technology in CAR-T cell therapy: a state-of-the-art review. Front Oncol 2024; 14:1388475.

1093 62. Kath J, Du W, Pruene A, Braun T, Thommandru B, Turk R, Sturgeon ML, Kurgan GL, Amini L, Stein M, et
1094 al. Pharmacological interventions enhance virus-free generation of *TRAC*-replaced CAR T cells. Mol
1095 Ther - Methods Clin Dev 2022; 25:311–30.

1096 63. Wagner DL, Koehl U, Chmielewski M, Scheid C, Stripecke R. Review: Sustainable Clinical Development
1097 of CAR-T Cells – Switching From Viral Transduction Towards CRISPR-Cas Gene Editing. Front Immunol
1098 2022; 13:865424.

1099 64. Glaser V, Flugel C, Kath J, Du W, Drosdek V, Franke C, Stein M, Pruß A, Schmueck-Henneresse M, Volk
1100 H-D, et al. Combining different CRISPR nucleases for simultaneous knock-in and base editing prevents
1101 translocations in multiplex-edited CAR T cells. Genome Biol 2023; 24:89.

1102 65. Engel NW, Steinfeld I, Ryan D, Anupindi K, Kim S, Wellhausen N, Chen L, Wilkins K, Baker DJ, Rommel
1103 PC, et al. Quadruple adenine base–edited allogeneic CAR T cells outperform CRISPR/Cas9 nuclease–
1104 engineered T cells. Proc Natl Acad Sci 2025; 122:e2427216122.

1105 66. Rossi M, Steklov M, Huberty F, Nguyen T, Marijsse J, Jacques-Hespel C, Najm P, Lonez C, Breman E.
1106 Efficient shRNA-based knockdown of multiple target genes for cell therapy using a chimeric miRNA
1107 cluster platform. Mol Ther - Nucleic Acids 2023; 34.

1108 67. Hamilton JR, Chen E, Perez BS, Sandoval Espinoza CR, Kang MH, Trinidad M, Ngo W, Doudna JA. In vivo
1109 human T cell engineering with enveloped delivery vehicles. Nat Biotechnol 2024; 42:1684–92.

1110 68. Zhao Y, Chen J, Andreatta M, Feng B, Xie Y-Q, Wenes M, Wang Y, Gao M, Hu X, Romero P, et al. IL-10-
1111 expressing CAR T cells resist dysfunction and mediate durable clearance of solid tumors and
1112 metastases. Nat Biotechnol 2024; 42:1693–704.

1113 69. Jaspers JE, Khan JF, Godfrey WD, Lopez AV, Ciampricotti M, Rudin CM, Brentjens RJ. IL-18–secreting
1114 CAR T cells targeting DLL3 are highly effective in small cell lung cancer models. J Clin Invest 2023; 133.

1115 70. Patel RP, Ghilardi G, Zhang Y, Chiang Y-H, Xie W, Guruprasad P, Kim KH, Chun I, Angelos MG, Pajarillo
1116 R, et al. CD5 deletion enhances the antitumor activity of adoptive T cell therapies. Sci Immunol 2024;
1117 9:eadn6509.

1118 71. Skopek R, Palusińska M, Kaczor-Keller K, Pingwara R, Papierniak-Wyglądała A, Schenk T, Lewicki S,
1119 Zelent A, Szymański Ł. Choosing the Right Cell Line for Acute Myeloid Leukemia (AML) Research. Int J
1120 Mol Sci 2023; 24:5377.

1121 72. Liu R, Wei H, Gao P, Yu H, Wang K, Fu Z, Ju B, Zhao M, Dong S, Li Z, et al. CD47 promotes ovarian cancer
1122 progression by inhibiting macrophage phagocytosis. Oncotarget 2017; 8:39021–32.

1123 73. De Vlieghere E, Carlier C, Ceelen W, Bracke M, De Wever O. Data on in vivo selection of SK-OV-3 Luc
1124 ovarian cancer cells and intraperitoneal tumor formation with low inoculation numbers. Data Brief
1125 2016; 6:542–9.

1126 74. Hsiau T, Conant D, Rossi N, Maures T, Waite K, Yang J, Joshi S, Kelso R, Holden K, Enzmann BL, et al.
1127 Inference of CRISPR Edits from Sanger Trace Data. 2019.

1128 75. Rvk- CN. Phoenix ™ Retrovirus Expression System. Phoenix Usa 4436:1–13.

1129 76. Laroy W, Contreras R, Callewaert N. Glycome mapping on DNA sequencing equipment. Nat Protoc
1130 2006; 1:397–405.

1131 77. Yang M, Tang X, Zhang Z, Gu L, Wei H, Zhao S, Zhong K, Mu M, Huang C, Jiang C, et al. Tandem CAR-T
1132 cells targeting CD70 and B7-H3 exhibit potent preclinical activity against multiple solid tumors.
1133 Theranostics 2020; 10:7622–34.

1134 78. R Core Team. A Language and environment for statistical computing. 2024; Available from:
1135 https://www.R-project.org/

1136 79. Hothorn T, Bretz F, Westfall P. Simultaneous Inference in General Parametric Models. Biom J 2008;
1137 50:346–63.

1138 80. Zeileis A. Econometric Computing with HC and HAC Covariance Matrix Estimators. J Stat Softw 2004;
1139 11:1–17.

1140 81. Zeileis A, Köll S, Graham N. Various Versatile Variances: An Object-Oriented Implementation of
1141 Clustered Covariances in R. J Stat Softw 2020; 95:1–36.

1142 82. Rizopoulos D. Generalized Linear Mixed Models using Adaptive Gaussian Quadrature. 2022; Available
1143 from: https://CRAN.R-project.org/package=GLMMadaptive

1144 83. Brooks ME, Kristensen K, Benthem KJ van, Magnusson A, Berg CW, Nielsen A, Skaug HJ, Mächler M,
1145 Bolker BM. glmmTMB Balances Speed and Flexibility Among Packages for Zero-inflated Generalized
1146 Linear Mixed Modeling. R J 2017; 9:378–400.

1147 84. Hothorn T, Bretz F, Westfall P. Simultaneous Inference in General Parametric Models.

1148 85. Therneau T. A Package for Survival Analysis in R. 2022; Available from: https://CRAN.R-
1149 project.org/package=survival

1150 86. Therneau T, Grambsch P. Modeling Survival Data: Extending the Cox Model. 2000;

1151 87. Kassambra A, Kosinski M, Biecek P. Survminer: Drawing Survival Cuvres using "ggplot2". 2021;
1152 Available from: https://CRAN.R-project.org/package=survminer

1153 88. Stuart T, Butler A, Hoffman P, Hafemeister C, Papalexi E, Mauck WM, Hao Y, Stoeckius M, Smibert P,
1154 Satija R. Comprehensive integration of single-cell data. Cell 2019; 177:1888-1902.e21.

1155 89. Xu S, Hu E, Cai Y, Xie Z, Luo X, Zhan L, Tang W, Wang Q, Liu B, Wang R, et al. Using clusterProfiler to
1156 characterize multiomics data. Nat Protoc 2024; 19:3292–320.

1157 90. Yu G, He Q-Y. ReactomePA: an R/Bioconductor package for reactome pathway analysis and
1158 visualization. Mol Biosyst 2016; 12:477–9.

1159 91. Kuleshov MV, Jones MR, Rouillard AD, Fernandez NF, Duan Q, Wang Z, Koplev S, Jenkins SL, Jagodnik
1160 KM, Lachmann A, et al. Enrichr: a comprehensive gene set enrichment analysis web server 2016
1161 update. Nucleic Acids Res 2016; 44:W90–7.

Figures

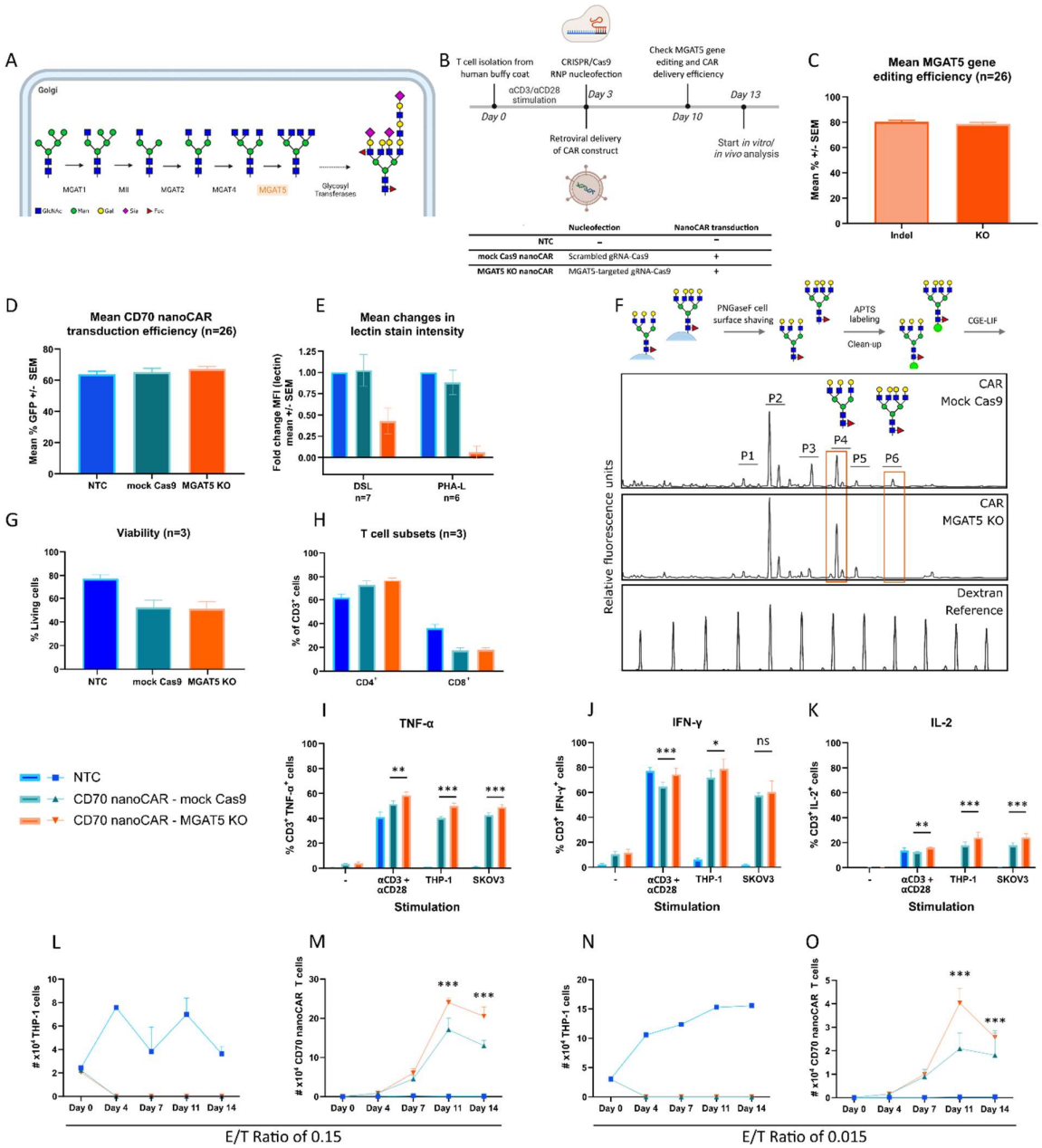
A
Golgi
MGAT1
MII
MGAT2
MGAT4
MGAT5
Glycosyl Transferases
B
T cell isolation from human buffy coat
CRISPR/Cas9 RNP nucleofection
Check MGAT5 gene editing and CAR delivery efficiency
αCD3/αCD28 stimulation
Day 0
Day 3
Day 10
Day 13
Retroviral delivery of CAR construct
Start in vitro/ in vivo analysis
Nucleofection
NanoCAR transduction
NTC
mock Cas9 nanoCAR
Scrambled gRNA-Cas9
MGAT5 KO nanoCAR
MGAT5-targeted gRNA-Cas9
C
Mean MGAT5 gene editing efficiency (n=26)
Mean % +/- SEM
Indel
KO
D
Mean CD70 nanoCAR transduction efficiency (n=26)
Mean % GFP +/- SEM
NTC
mock Cas9
MGAT5 KO
E
Mean changes in lectin stain intensity
Fold change MFI (lectin) mean +/- SEM
DSL n=7
PHA-L n=6
F
PNGaseF cell surface shaving
APTS labeling
Clean-up
CGE-LIF
CAR Mock Cas9
CAR MGAT5 KO
Dextran Reference
Relative fluorescence units
P1
P2
P3
P4
P5
P6
G
Viability (n=3)
% Living cells
H
T cell subsets (n=3)
% of CD3+ cells
CD4+
CD8+
NTC
CD70 nanoCAR - mock Cas9
CD70 nanoCAR - MGAT5 KO
I
TNF-α
% CD3+ TNF-α+ cells
J
IFN-γ
% CD3+ IFN-γ+ cells
K
IL-2
% CD3+ IL-2+ cells
Stimulation
L
M
N
O
x10⁴ THP-1 cells
x10⁴ CD70 nanoCAR T cells
Day 0
Day 4
Day 7
Day 11
Day 14
E/T Ratio of 0.15
E/T Ratio of 0.015

1170 **Figure 1 | *MGAT5* glyco-gene editing and CD70 nanoCAR engineering and the impact of glyco-engineering in**
1171 ***MGAT5* on *in vitro* CD70 nanoCAR efficacy. A.** Pathway of N-glycan branching. N-glycan branching is
1172 achieved through a series of mannosidase (M) and mannosylglycoprotein-N-acetylglucosaminyltransferase
1173 (MGAT)-mediated reactions. MGAT5, the enzyme of interest to our project is marked in orange. This
1174 branching primarily occurs in the medial-Golgi compartment. In later compartments, branched glycans are
1175 further modified by other enzymes including Gal-, GlcNAc-, sialyl- and fucosyltransferases to result in
1176 complex glycans. **B.** Experimental timeline. **C.** Mean editing efficiency as % insertions/deletions (indels) or
1177 proportion of indels that result in a frameshift or are 21+ bp in length (assumes all edits are in a coding
1178 region) (KO) obtained for the *MGAT5* locus. n=26, SEM: standard error of the mean. **D.** Mean transduction
1179 efficiency as % GFP expressing cells for the different engineering conditions. n=26, **E and F.** Profiling of
1180 alterations in cell surface glycosylation upon *MGAT5* KO in CD70 nanoCAR T cells. **E.** Lectin staining. 2 x 10^5
1181 wild type, mock-engineered (green) or *MGAT5* KO (orange) CAR T cells were collected, stained with fixable
1182 viability dye eFl780 and biotinylated lectin from *Datura stramonium* (DSL) or phytohemagglutinin-L lectin
1183 (PHA-L) followed by secondary staining with PE-coupled neutravidin. Analysis was done by flow cytometry
1184 and graphs show the mean reduction in lectin binding signal intensities as compared to wild type CAR T
1185 cells after gating on viable cells. Results are shown for engineered T cells from 7 (DSL)/6 (PHA-L)
1186 independent blood donors. **F.** CGE-LIF profiling. Schematic representation of the sample preparation and
1187 CGE-LIF profiles of the cell-surface glycome of mock-engineered and MGAT5 KO CD70 nanoCAR T cells.
1188 Sialidase digest was performed on the samples prior to the analysis. The major pairs of peaks in the profile
1189 are annotated P1-P6, based on the profile of total human plasma glycoprotein N-glycans which was run as
1190 a reference. The N-glycan profile of MGAT5 KO CD70 nanoCAR T cells is clearly different from that of mock-
1191 engineered CAR T cells. The peaks in P6 disappear while the peaks in P4 show a higher intensity relative to
1192 P2 and P3. This shift in electrophoretic mobility is consistent with the removal of one LacNAc unit (two
1193 monosaccharide units) or a shift from a tetra-antennary to a tri-antennary N-glycan. **G.** and **H.** Effect of
1194 *MGAT5* KO on CD70 nanoCAR viability and subset distribution at day 13 of *in vitro* culturing. At day 13, the
1195 immunophenotype of the cells was evaluated prior to the initiation of the functional assays. Mean data is
1196 shown from experiments performed with three independent donors. Error bars represent the SEM. **I-K.**
1197 The impact of glyco-engineering of *MGAT5* on *in vitro* CD70 nanoCAR cytokine production. Cytokine
1198 production of glyco-engineered CD70 nanoCAR T cells was evaluated by intracellular staining after co-
1199 incubation with THP-1 and SKOV-3 target cell lines for 16 hours. Unstimulated cells were included as
1200 negative control (-) while Immunocult stimulation was included as positive control (+). Technical duplicates
1201 were analyzed. The bars show the mean fractions of TNF-α, IFN-γ and IL-2 positive $CD3^+$ obtained from
1202 three independent donors. Error bars represent the standard deviation. **L-O**. The impact of glyco-
1203 engineering in *MGAT5* on *in vitro* CD70 nanoCAR cytotoxic potential. Glyco-engineered CD70 nanoCAR T
1204 cells cultured in the presence of IL-7 and IL-15 were incubated at different effector to target THP-1 cell
1205 ratios (E/T) in technical duplicates and cell numbers were analyzed over a time period of 14 days. A second
1206 challenge with THP-1 cells was added at day 7. Error bars represent the SEM on cell number from data
1207 obtained with 3 different T cell donors. **L** and **M**. Results for E/T ratio of 0.15 corresponding to the co-
1208 culture of 20 000 THP-1 cells with 3 000 glyco-engineered CD70 nanoCAR T cells. **N** and **O**. Results for E/T
1209 ratio of 0.015 corresponding to the co-culture of 20 000 THP-1 cells with 300 CD70 nanoCAR T cells. To
1210 account for the correlation over time, the data from panels **M** and **O** was modeled using a mixed negative
1211 binomial model with a random intercept for each cluster (a cluster being defined as the set of
1212 measurements sharing the same donor, E/T Ratio and type of CAR T cells). We found that, on day 11, the
1213 number of *MGAT5* KO nanoCAR T cells is about 1.74 times higher (95% CI: 1.36 to 2.21) than the number
1214 of nanoCAR T cells starting from the same conditions. On day 14, the number of *MGAT5* KO nanoCAR T

similarly is about 1.70 times higher (95% CI: 1.33 to 2.18). All these estimates are averaged over the two E/T ratios and the three independent donors; *** $p < 0.001$, ** $0.001 < p < 0.01$, * $0.01 < p < 0.05$, ns $p > 0.05$

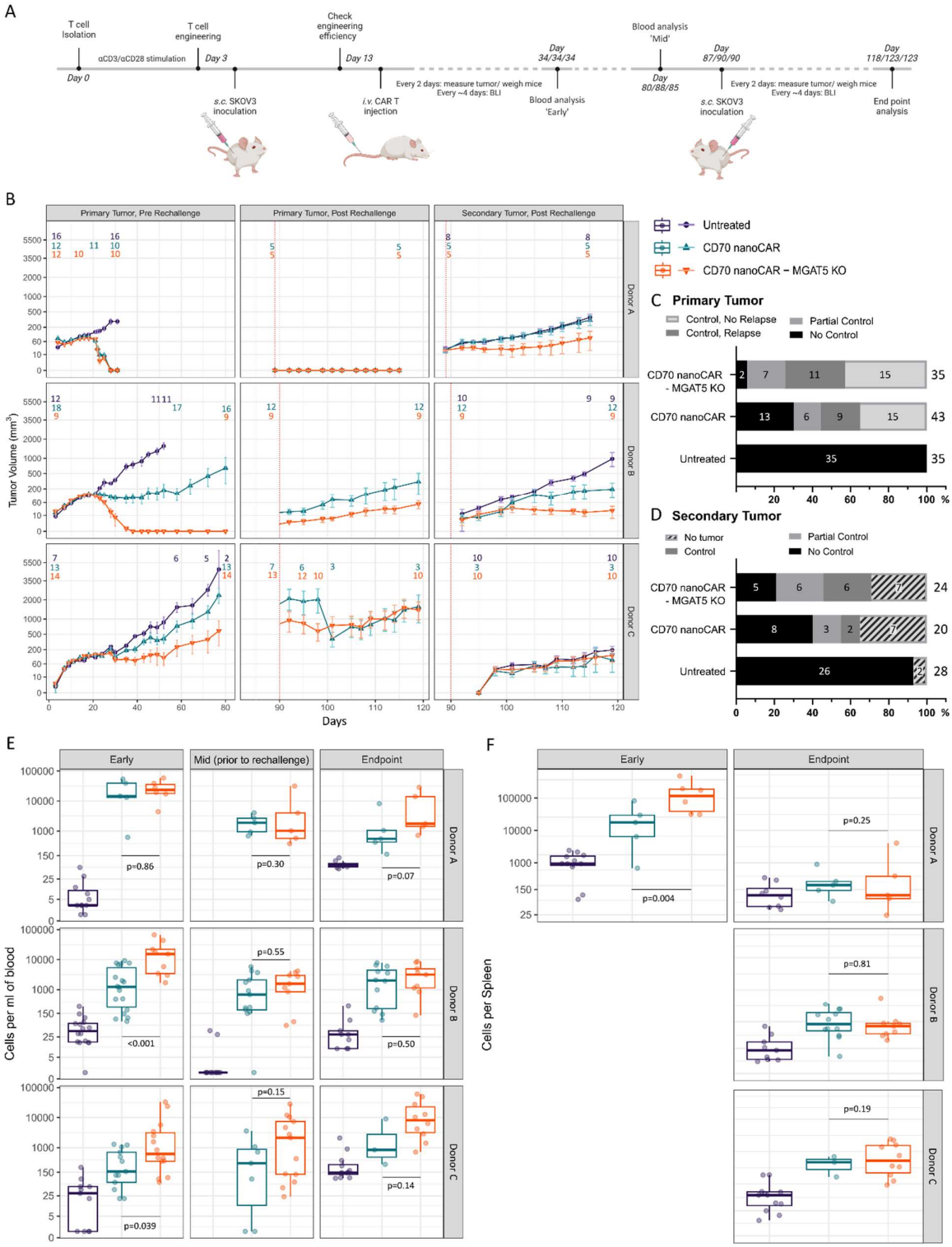
A
T cell Isolation
Day 0
αCD3/αCD28 stimulation
T cell engineering
Day 3
s.c. SKOV3 inoculation
Check engineering efficiency
Day 13
i.v. CAR T injection
Every 2 days: measure tumor/ weigh mice
Every ~4 days: BLI
Day 34/34/34
Blood analysis 'Early'
Blood analysis 'Mid'
Day 80/88/85
Day 87/90/90
s.c. SKOV3 inoculation
Every 2 days: measure tumor/ weigh mice
Every ~4 days: BLI
Day 118/123/123
End point analysis
B
Primary Tumor, Pre Rechallenge
Primary Tumor, Post Rechallenge
Secondary Tumor, Post Rechallenge
Donor A
Donor B
Donor C
Tumor Volume (mm³)
Days
Untreated
CD70 nanoCAR
CD70 nanoCAR – MGAT5 KO
C Primary Tumor
Control, No Relapse
Control, Relapse
Partial Control
No Control
CD70 nanoCAR - MGAT5 KO
CD70 nanoCAR
Untreated
D Secondary Tumor
No tumor
Control
Partial Control
No Control
E
Early
Mid (prior to rechallenge)
Endpoint
Cells per ml of blood
p=0.86
p=0.30
p=0.07
p=0.55
<0.001
p=0.50
p=0.15
p=0.039
p=0.14
F
Cells per Spleen
p=0.004
p=0.25
p=0.81
p=0.19

1220 **Figure 2 | The impact of glyco-engineering on *in vivo* CD70 nanoCAR functionality in the SKOV-3 solid tumor**
1221 **model**. **A.** Schematic representation of the experimental timeline for the study of the *in vivo* efficacy of
1222 MGAT5 KO CD70 nanoCAR T cells. **B.** Mean tumor burden measured by caliper. Tumor volume is calculated
1223 as (tumor length x tumor width^2)/2. Group means are indicated with error bars representing the SEM.
1224 Original values of tumor volume are shown, Y-axis is cube root transformed. Number of mice surviving in
1225 each group are indicated above the datapoints and adapted at timepoints whenever a mouse was
1226 sacrificed at humane endpoint. Timepoint of rechallenge is indicated with at dashed red line. **C.** Overview
1227 of the response to primary tumor challenge in the different treatment groups for all three experiments
1228 combined. **D.** Overview of the response to secondary tumor challenge in the different treatment groups
1229 for all three experiments combined. **E and F.** Number of CAR T cells identified in the different treatment
1230 conditions in peripheral blood (E) and spleen (F) at day 34/34/34 (Early), day 80/88/85 (Mid) and day
1231 118/123/123 (Endpoint) in three independent experiments with cells derived from donors A/B/C. Data is
1232 represented as concentration of $CD3^+GFP^+$ cells per ml of blood or per spleen. The number of CAR T cells
1233 in the spleen is counted based on a gating strategy that includes both $CD4^+$ and $CD8^+$ T cells. Each data
1234 point represents a single animal. The difference between groups was tested using a quasi-Poisson GLM at
1235 each timepoint and for each donor, p-values are indicated within the respective plots.

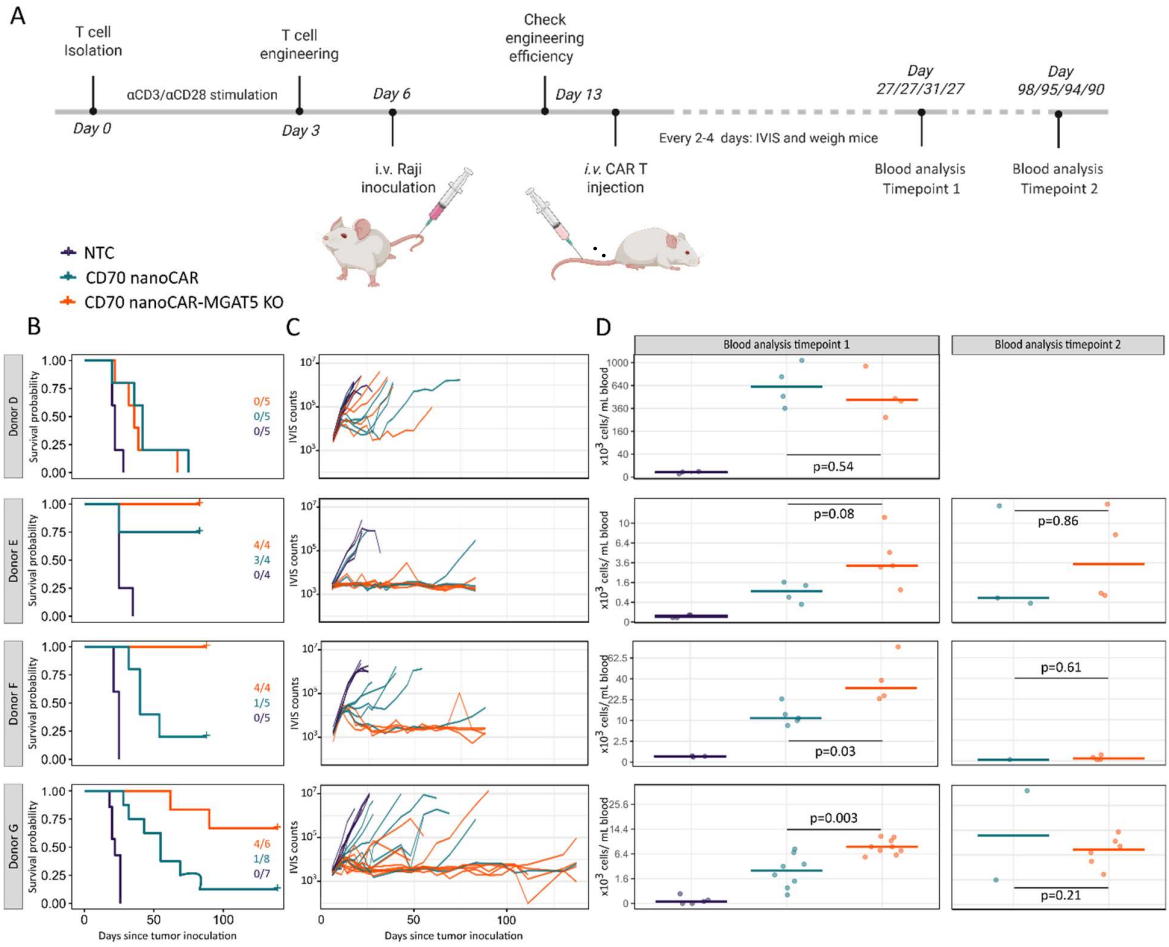

Figure 3 | The impact of *MGAT 5* KO on *in vivo* CD70 nanoCAR functionality in the Raji lymphoma model. A. Schematic representation of the experimental timeline for the study of the *in vivo* efficacy of MGAT5 KO CD70 nanoCAR T cells. **B** Kaplan-Meier survival curves for CD70 nanoCAR treated mice. The number of surviving mice at the end of the experiment vs. the number of mice per group at the start of the experiment are indicated. Data from 4 independent donors (D, E, F, G) are shown. **C.** Bioluminescence imaging of tumor burden in all mice individually. IVIS counts are total whole-body counts measured as photons/sec. **D.** Flow cytometry-based analysis of CD70 nanoCAR T cells in blood**.** Number of CAR T cells identified in the different treatment conditions in peripheral blood at day 27/27/31/27 (Timepoint 1) and day 98/95/94/90 (Timepoint 2), in four independent experiments with cells derived from donors D/E/F/G. CAR T cells were detected as human $CD3^{+}GFP^{+}$ cells. Each data point represents a single animal. The number of CAR T cells present in the blood is indicated as cells/mL blood. The difference between groups was tested using a quasi-Poisson GLM at each timepoint and for each donor, p-values are indicated within the respective plots.

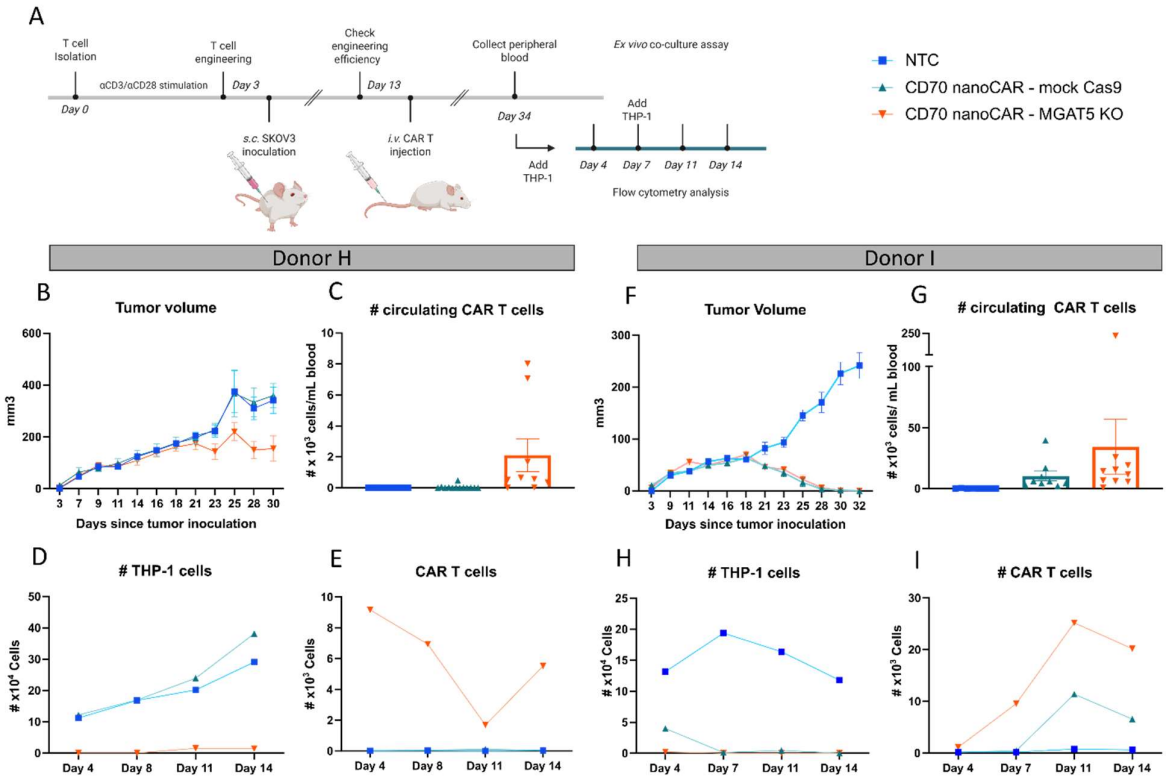

Figure 4| The impact of glyco-engineering in *MGAT5* on *ex vivo* CD70 nanoCAR efficacy. A. Time line of the experiment. Data obtained for cells engineered from donor H (panel B-E) and donor I (panel F-I). **B and F.** SKOV-3 tumor burden measured by caliper. Tumor volume is calculated as (tumor length x tumor width2)/2. Group means are indicated with error bars representing the SEM. **C and G.** The number of CD70 nanoCAR T cells (represented as number of $CD3^{+}GFP^{+}$ cells) present in the blood is indicated as cells/mL blood. Each data point represents a single animal. Error bars represent the SEM. **D-E** and **H-I.** The impact of glyco-engineering in *MGAT5* on *ex vivo* CD70 nanoCAR cytotoxic potential. Blood was prepared from SKOV-3 tumor bearing mice 21 days after treatment with either WT or MGAT5 KO CD70 nanoCAR T cells. Cells prepared from 50µL blood (donor H) or 40µL blood (donor I) were put in co-culture with 20 000 THP-1 cells and THP-1 and CAR T cell counts were followed over a time period of 14 days. A second challenge with THP-1 cells was added at day 7.

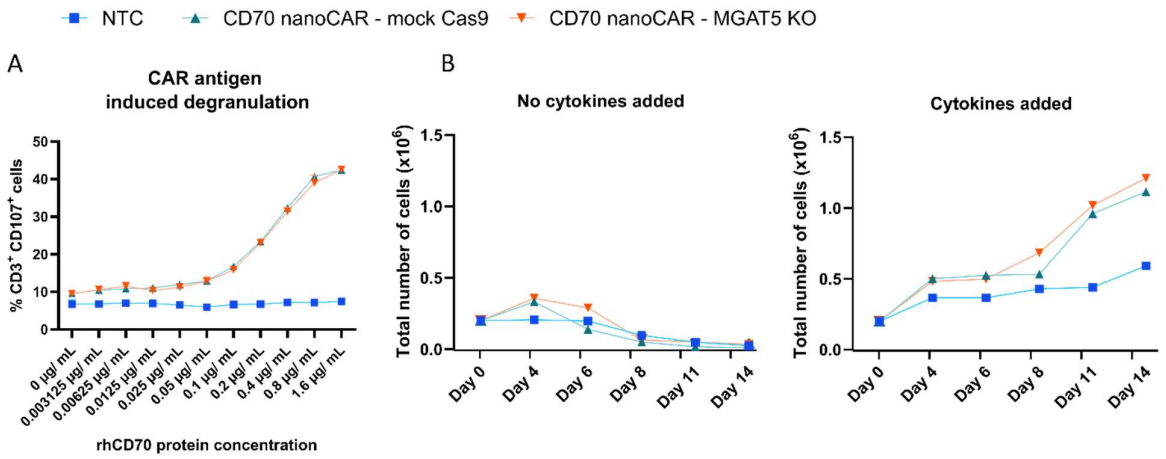

Figure 5| MGAT5 KO CD70 nanoCAR T cells require equal antigen density to degranulate and fully depend on cytokine growth factors for their proliferation. A. Flow cytometry analysis of CD107a degranulation assay, on cells from donor K. Untransduced T cells (NTC) and CD70 nanoCAR T cells with and without *MGAT5* engineering were co-cultured in technical duplicate with different concentrations (3.125 ng/ mL up to 1.6 µg/ mL) of coated rhCD70 protein for 5 hours. $CD107a^+$ cell staining was analyzed by flow cytometry gating on $CD3^+$ cells. Data shown is representative of three experiments performed with T cells obtained from two independent donors. **B.** Cytokine independent growth assay performed on cells engineered and cultured in the presence of IL-7 and IL-15 as described in the engineering protocol (from donor G). Left, total T cell count of engineered T cells cultured in the presence IL-7 and IL-15 for an additional 14 days. Right, total T cell count of engineered T cells cultured in the absence of supplemental cytokines.

1274

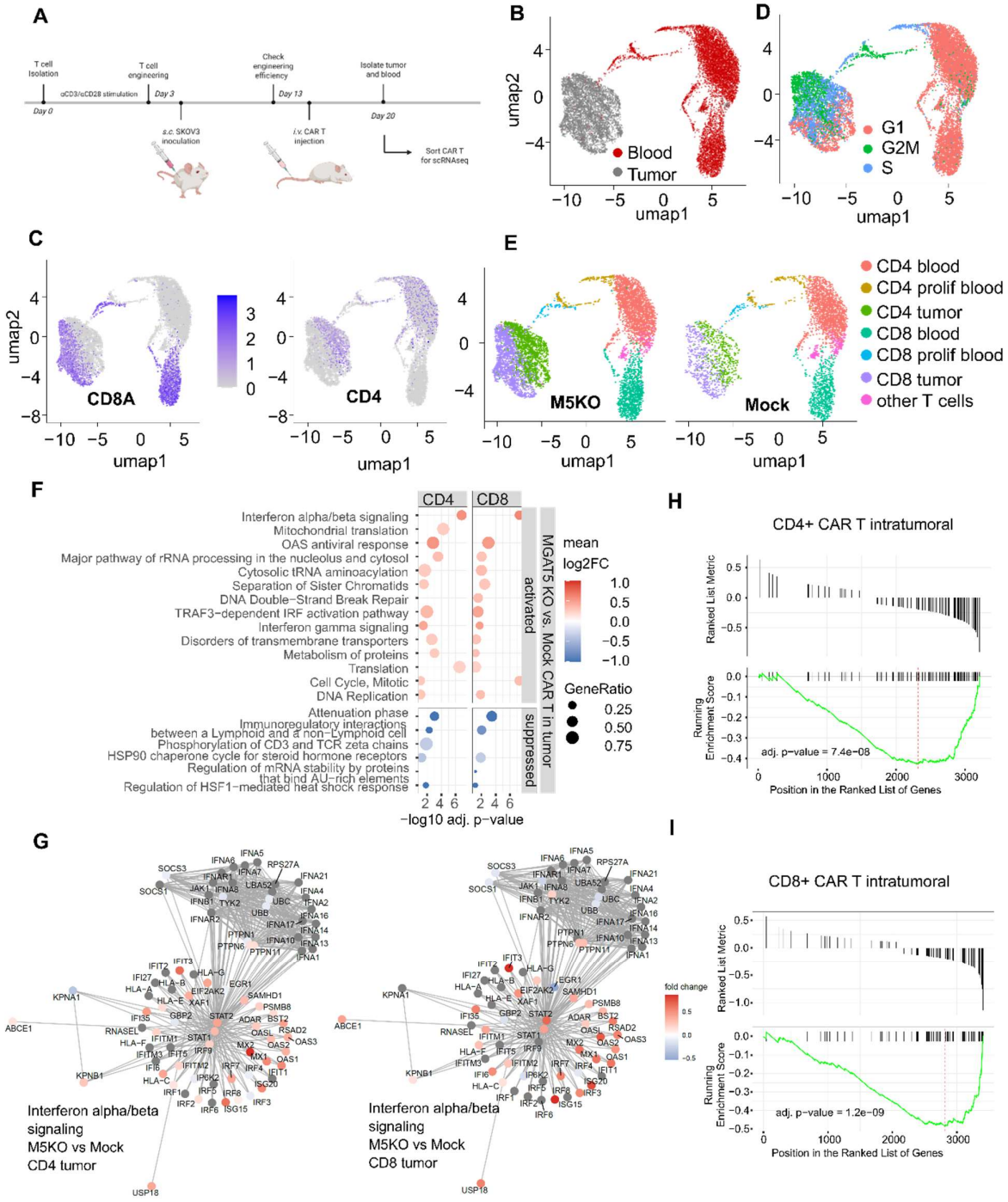

1275
1276

1277 **Figure 6| Single cell RNA sequencing of tumor-infiltrating and circulating CAR T cells. A.** Experiment outline,
1278 performed on donor J. Dimensionality reduction and clustering of cells was driven by key biological
1279 differences. **B.** Sample origin, **C.** lymphocyte type and **D.** cell cycle state, leading to the distinction of 7 cell
1280 populations as depicted in panel **E. F.** Gene set enrichment analysis of Reactome pathways and **(G)**
1281 significantly upregulated interferon alpha/beta signaling, compared to control CAR T cells. Genes not
1282 included in differential expression analysis (expressed in fewer than 25% of cells or showing log2 fold
1283 change < 0.1) were marked in grey **H-I.** Gene set enrichment analysis showed significant overlap between
1284 our results (CD4 tumor, panel H; CD8 tumor, panel I) and previously published genes implicated in CAR T
1285 cell exhaustion[42]. The running enrichment score is calculated by traversing our ranked list of genes,
1286 increasing a running sum when a gene from the tested set is encountered and decreasing when a gene
1287 outside the set is encountered. The enrichment score (dashed red line) is the maximum deviation of this
1288 running sum from zero.

1289 # Supplementary information

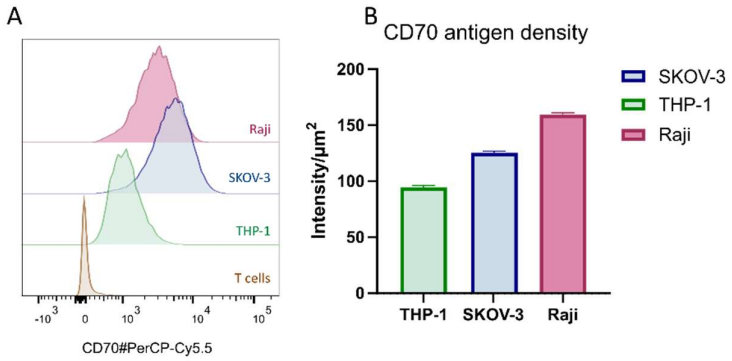

1290

1291 **Supplementary Figure 1 | Characterization of the SKOV-3, THP-1 and Raji cell lines used as target cells. A.**
1292 CD70 antigen expression on the THP-1 and SKOV-3 target cell lines was evaluated by flow cytometry. Jurkat
1293 cells were included as negative control. Non-transduced control (NTC) and CD70 nanoCAR expressing
1294 human T cells were included to check for auto-antigen expression. **B.** CD70 antigen density on SKOV-3,
1295 THP-1 and Raji target cell lines was evaluated by multispectral imaging flow cytometry. Antigen density is
1296 represented as mean fluorescence intensity/ μm^2. Error bars represent the 95% confidence interval.

1297

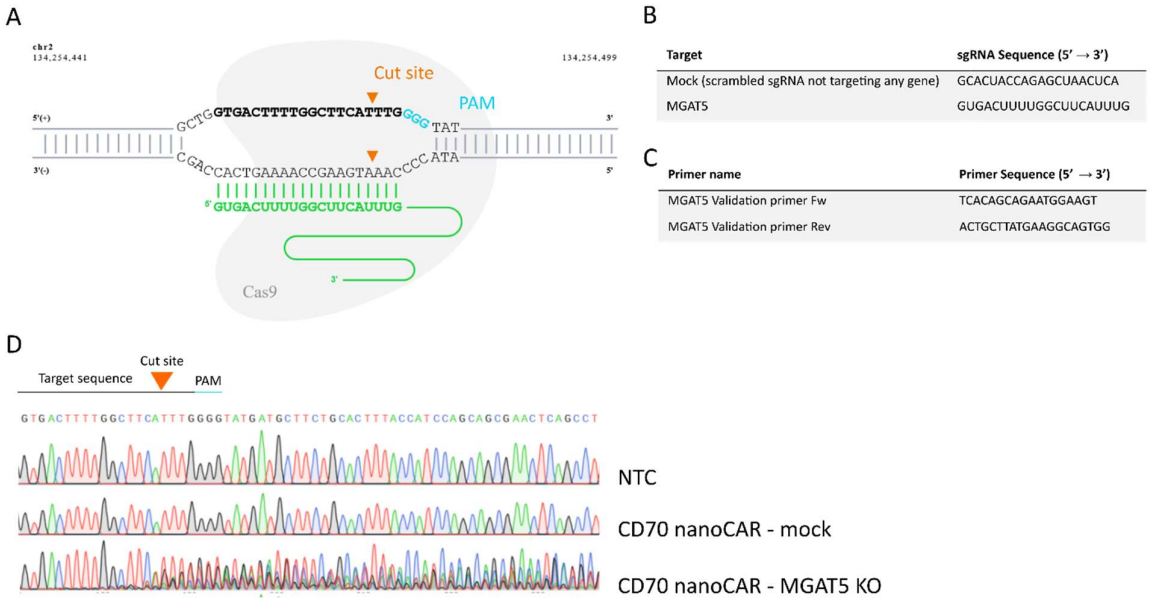

Target	sgRNA Sequence (5′ → 3′)
Mock (scrambled sgRNA not targeting any gene)	GCACUACCAGAGCUAACUCA
MGAT5	GUGACUUUUGGCUUCAUUUG

Primer name	Primer Sequence (5′ → 3′)
MGAT5 Validation primer Fw	TCACAGCAGAATGGAAGT
MGAT5 Validation primer Rev	ACTGCTTATGAAGGCAGTGG

1298

1299 **Supplementary Figure 2| A.** Genome localization of the gRNA target site (green) with indication of the PAM
1300 (blue) and the predicted Cas9 cut site (orange) **B.** Overview of the gRNA used in this study to generate a
1301 knockout in *MGAT5* **C.** PCR primers to amplify the CRISPR target site. The forward primers were used for
1302 Sanger sequencing. **D.** Sequencing data of NTC, Mock Cas9 and MGAT5 KO CD70 nanoCAR T cells. *MGAT5*-
1303 targeting sgRNA sequence with its PAM and Cut site are indicated in the sequence.

1304

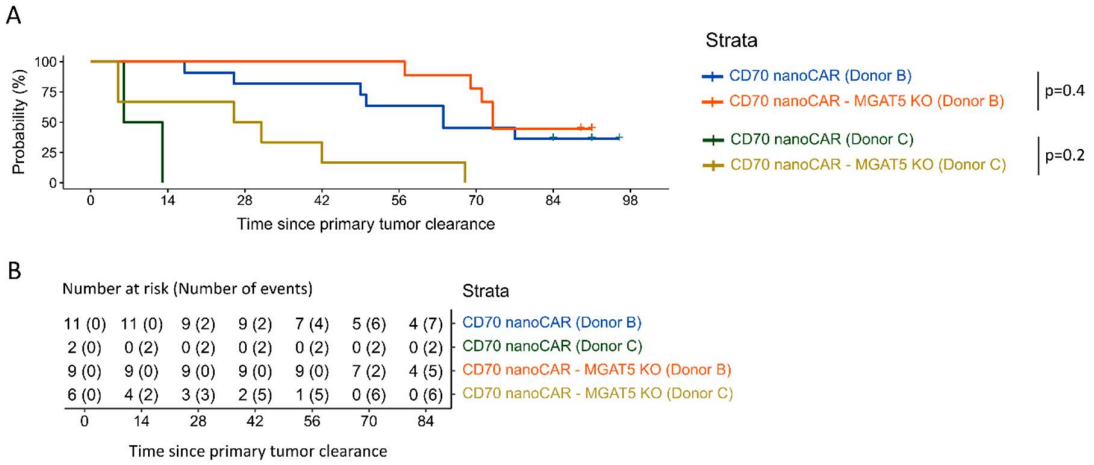

1305

1306 **Supplementary Figure 3 | Time (in days) to relapse of the primary tumor** (Experiment with donor B/C, not
1307 for donor A, as no primary tumor relapse occurred in CAR T treated mice, see **Figure 2**.B). Time zero was
1308 set as the time that the primary tumor was undetectable or partially controlled. Relapse event was defined
1309 at the time at which the tumor starts growing again. As the onset of relapse, we take the first day that the
1310 tumor volume reaches again > 4 mm^3 and only when tumor growth is also seen in 4 consecutive
1311 measurement days following that day. **A.** Kaplan-Meier curve. This plot shows the probability of relapse-
1312 free survival in the two groups. **B.** Risk and event table corresponding to the Kaplan-Meier plot. The table
1313 shows the number of mice at risk and, between brackets, the cumulative number of relapses in each group
1314 and at each time.

Primary Tumor (Donor A)

A

Parameter	estimate	std.error	statistic	p.value
(Intercept)	3.808	0.166	22.942	1.8E-116
ns(Day, df = 5)1	0.834	0.156	5.360	8.32E-08
ns(Day, df = 5)2	0.910	0.150	6.064	1.33E-09
ns(Day, df = 5)3	1.350	0.126	10.735	6.98E-27
ns(Day, df = 5)4	2.148	0.291	7.374	1.66E-13
ns(Day, df = 5)5	1.471	0.099	14.894	3.61E-50
GroupCD70 nanoCAR	0.159	0.252	0.631	0.52791
GroupCD70 nanoCAR - MGAT5 KO	-0.079	0.259	-0.305	0.760337
ns(Day, df = 5)1:GroupCD70 nanoCAR	-0.106	0.249	-0.426	0.670121
ns(Day, df = 5)2:GroupCD70 nanoCAR	-1.019	0.324	-3.147	0.001648
ns(Day, df = 5)3:GroupCD70 nanoCAR	-4.533	0.682	-6.643	3.08E-11
ns(Day, df = 5)4:GroupCD70 nanoCAR	-8.097	1.623	-4.990	6.04E-07
ns(Day, df = 5)5:GroupCD70 nanoCAR	-10.073	2.784	-3.619	0.000296
ns(Day, df = 5)1:GroupCD70 nanoCAR - MGAT5 KO	-0.006	0.264	-0.023	0.981813
ns(Day, df = 5)2:GroupCD70 nanoCAR - MGAT5 KO	-0.313	0.340	-0.922	0.356772
ns(Day, df = 5)3:GroupCD70 nanoCAR - MGAT5 KO	-6.696	0.805	-8.319	8.86E-17
ns(Day, df = 5)4:GroupCD70 nanoCAR - MGAT5 KO	-7.682	1.292	-5.944	2.78E-09
ns(Day, df = 5)5:GroupCD70 nanoCAR - MGAT5 KO	-8.299	2.116	-3.923	8.76E-05
Random intercept S.D. (ID:mouse)	0.483			

B

Contrast	Estimate	95% CI, lower	95% CI, upper	Adj. p-value
Ratio of CD70 nanoCAR over MGAT5 KO CD70 nanoCAR tumor sizes at day 0	1.534	0.363	6.482	0.756
Ratio of CD70 nanoCAR over MGAT5 KO CD70 nanoCAR tumor sizes at day 30	0.433	0.001	191.034	0.942

Secondary Tumor (Donor A)

C

Parameter	estimate	std.error	statistic	p.value
(Intercept)	3.084	0.427	7.230	4.82703E-13
ns(Day, df = 5)1	1.012	0.329	3.081	0.002061141
ns(Day, df = 5)2	1.654	0.358	4.623	3.77679E-06
ns(Day, df = 5)3	1.867	0.239	7.799	6.22111E-15
ns(Day, df = 5)4	3.319	0.582	5.701	1.19362E-08
ns(Day, df = 5)5	2.159	0.165	13.071	4.83752E-39
GroupCD70 nanoCAR	0.083	0.680	0.122	0.902898573
GroupCD70 nanoCAR - MGAT5 KO	-0.325	0.689	-0.472	0.636833056
ns(Day, df = 5)1:GroupCD70 nanoCAR	-0.145	0.525	-0.276	0.782746661
ns(Day, df = 5)2:GroupCD70 nanoCAR	-0.303	0.575	-0.528	0.597663013
ns(Day, df = 5)3:GroupCD70 nanoCAR	-0.245	0.387	-0.634	0.526288616
ns(Day, df = 5)4:GroupCD70 nanoCAR	-0.387	0.916	-0.423	0.672444085
ns(Day, df = 5)5:GroupCD70 nanoCAR	-0.333	0.267	-1.247	0.212296446
ns(Day, df = 5)1:GroupCD70 nanoCAR - MGAT5 KO	-1.764	0.668	-2.638	0.008336857
ns(Day, df = 5)2:GroupCD70 nanoCAR - MGAT5 KO	-1.736	0.729	-2.383	0.017191083
ns(Day, df = 5)3:GroupCD70 nanoCAR - MGAT5 KO	-1.702	0.524	-3.252	0.00114661
ns(Day, df = 5)4:GroupCD70 nanoCAR - MGAT5 KO	-2.296	0.978	-2.347	0.018904292
ns(Day, df = 5)5:GroupCD70 nanoCAR - MGAT5 KO	-1.516	0.351	-4.325	1.52666E-05
Random intercept S.D. (ID:mouse)	0.968			

D

Contrast	Estimate	95% CI, lower	95% CI, upper	Adj. p-value
Ratio of CD70 nanoCAR over MGAT5 KO CD70 nanoCAR tumor sizes at day 89	1.505	0.292	7.765	0.773
Ratio of CD70 nanoCAR over MGAT5 KO CD70 nanoCAR tumor sizes at day 115	6.382	1.473	27.656	0.011

1317 **Supplementary Figure 4| Longitudinal analysis of donor A.** Using the longitudinal data of the primary and
1318 secondary tumors in experiment with donor A, a Tweedie GLMM (generalized linear mixed model) with log
1319 link was used to model the tumor volume of the primary tumor (A) and secondary tumor (C). Summary of
1320 the model output, listing all parameter estimates for the model TumorVol ~ ns(Day, df = 5)*Group + (1 |
1321 ID), ns = natural spline. The table gives parameters and standard errors on the natural log scale together
1322 with test statistics and multiple testing adjusted p-values (null hypothesis: parameter equal to zero). **B and**
1323 **D.** Inference for different research questions. In this table, the estimates and confidence intervals are
1324 transformed back to the original scale so we can interpret them as the ratio of the mean tumor volume in
1325 the WT over the MGAT5 KO group. In this context, the adjusted p-values also relate to a transformed null
1326 hypothesis (i.e. estimate equals one). S.E.: Standard Error. CI: Confidence Interval.

Primary Tumor (Donor B)

A

Parameter	estimate	std.error	statistic	p.value
(Intercept)	2.378	0.331	7.175	7.25672E-13
ns(Day, df = 5)1	2.794	0.434	6.440	1.19106E-10
ns(Day, df = 5)2	4.278	0.629	6.805	1.00707E-11
ns(Day, df = 5)3	3.948	0.938	4.209	2.56362E-05
ns(Day, df = 5)4	9.983	2.165	4.611	4.01235E-06
ns(Day, df = 5)5	9.271	3.188	2.908	0.003633128
GroupCD70 nanoCAR	0.481	0.413	1.166	0.243768941
GroupCD70 nanoCAR - MGAT5 KO	0.489	0.492	0.994	0.320287544
ns(Day, df = 5)1:GroupCD70 nanoCAR	-0.876	0.553	-1.584	0.1132357
ns(Day, df = 5)2:GroupCD70 nanoCAR	-4.057	0.810	-5.012	5.39496E-07
ns(Day, df = 5)3:GroupCD70 nanoCAR	-5.450	1.191	-4.577	4.72805E-06
ns(Day, df = 5)4:GroupCD70 nanoCAR	-9.127	2.472	-3.692	0.000222535
ns(Day, df = 5)5:GroupCD70 nanoCAR	-11.206	3.385	-3.311	0.000929654
ns(Day, df = 5)1:GroupCD70 nanoCAR - MGAT5 KO	-0.734	0.699	-1.050	0.293717277
ns(Day, df = 5)2:GroupCD70 nanoCAR - MGAT5 KO	-7.225	1.669	-4.329	1.50113E-05
ns(Day, df = 5)3:GroupCD70 nanoCAR - MGAT5 KO	-66.313	28.873	-2.297	0.021632878
ns(Day, df = 5)4:GroupCD70 nanoCAR - MGAT5 KO	-37.410	12.369	-3.024	0.002491709
ns(Day, df = 5)5:GroupCD70 nanoCAR - MGAT5 KO	-15.796	3.720	-4.246	2.17593E-05
Random intercept S.D. (ID=mouse)	0.908			
Random slope S.D. (ID=mouse)	0.058			
Correlation random intercept and slope	-0.894			

B

Contrast	Estimate	95% CI, lower	95% CI, upper	Adj. p-value
Ratio of CD70 nanoCAR over MGAT5 KO CD70 nanoCAR tumor sizes at day 0	1.008	0.276	3.677	1
Ratio of CD70 nanoCAR over MGAT5 KO CD70 nanoCAR tumor sizes at day 86	621.771	3.74	103364.619	0.01

Secondary Tumor (Donor B)

C

Parameter	estimate	std.error	statistic	p.value
(Intercept)	2.426	1.027	2.361	0.018227304
ns(Day, df = 5)1	1.936	0.572	3.388	0.000705151
ns(Day, df = 5)2	3.324	0.606	5.489	4.05082E-08
ns(Day, df = 5)3	3.070	0.393	7.814	5.52988E-15
ns(Day, df = 5)4	5.330	1.118	4.766	1.88006E-06
ns(Day, df = 5)5	3.396	0.321	10.570	4.12013E-26
GroupCD70 nanoCAR	-2.890	1.514	-1.908	0.056357932
GroupCD70 nanoCAR - MGAT5 KO	-3.146	1.762	-1.786	0.074173484
ns(Day, df = 5)1:GroupCD70 nanoCAR	0.801	0.958	0.836	0.403415871
ns(Day, df = 5)2:GroupCD70 nanoCAR	-0.996	0.984	-1.012	0.311431398
ns(Day, df = 5)3:GroupCD70 nanoCAR	0.085	0.670	0.127	0.898969154
ns(Day, df = 5)4:GroupCD70 nanoCAR	-2.541	1.800	-1.411	0.158160596
ns(Day, df = 5)5:GroupCD70 nanoCAR	-0.130	0.608	-0.213	0.831247718
ns(Day, df = 5)1:GroupCD70 nanoCAR - MGAT5 KO	0.435	1.221	0.356	0.721512015
ns(Day, df = 5)2:GroupCD70 nanoCAR - MGAT5 KO	-1.562	1.428	-1.094	0.273864409
ns(Day, df = 5)3:GroupCD70 nanoCAR - MGAT5 KO	-1.837	0.995	-1.846	0.064885039
ns(Day, df = 5)4:GroupCD70 nanoCAR - MGAT5 KO	-2.148	2.393	-0.897	0.36948293
ns(Day, df = 5)5:GroupCD70 nanoCAR - MGAT5 KO	-2.509	0.790	-3.175	0.001500741
Random intercept S.D. (ID=mouse)	2.868			

D

Contrast	Estimate	95% CI, lower	95% CI, upper	Adj. p-value
Ratio of CD70 nanoCAR over MGAT5 KO CD70 nanoCAR tumor sizes at day 92	1.292	0.028	60.081	0.98
Ratio of CD70 nanoCAR over MGAT5 KO CD70 nanoCAR tumor sizes at day 119	4.412	0.171	113.781	0.46

1328 **Supplementary Figure 5 | Longitudinal analysis of Donor B.** Longitudinal analysis of the primary (A-B) and
1329 secondary tumor (C-D). **A and C.** A Tweedie GLMM (generalized linear mixed model) with log link was used
1330 to model the tumor volume. A. Summary of the model output, listing all parameter estimates for the model
1331 TumorVol ~ ns(Day, df = 5)*Group + (Day | ID), ns = natural spline. The table gives parameters and standard
1332 errors on the natural log scale together with test statistics and multiple testing adjusted p-values (null
1333 hypothesis: parameter equal to zero). **B and D.** Inference for different research questions. In this table, the
1334 estimates and confidence intervals are transformed back to the original scale so we can interpret them in
1335 a straightforward way. Note: the estimate of 621.771 in panel B should be interpreted with caution, since
1336 within this contrast we are comparing to a tumor volume reaching zero. S.E.: Standard Error. CI: Confidence
1337 Interval.

Primary Tumor (Donor C)

A

Parameter	estimate	std.error	statistic	p.value
(Intercept)	3.605	0.381	9.452	3.32E-21
ns(Day, df = 5)1	1.296	0.368	3.521	0.00043
ns(Day, df = 5)2	2.396	0.391	6.127	8.95E-10
ns(Day, df = 5)3	3.008	0.290	10.379	3.1E-25
ns(Day, df = 5)4	5.081	0.674	7.540	4.71E-14
ns(Day, df = 5)5	4.198	0.243	17.288	5.78E-67
GroupCD70 nanoCAR	0.140	0.469	0.298	0.765351
GroupCD70 nanoCAR - MGAT5 KO	0.146	0.463	0.314	0.753514
ns(Day, df = 5)1:GroupCD70 nanoCAR	-0.294	0.455	-0.647	0.517655
ns(Day, df = 5)2:GroupCD70 nanoCAR	-0.849	0.487	-1.743	0.08127
ns(Day, df = 5)3:GroupCD70 nanoCAR	-1.237	0.362	-3.415	0.000637
ns(Day, df = 5)4:GroupCD70 nanoCAR	-0.855	0.820	-1.042	0.297185
ns(Day, df = 5)5:GroupCD70 nanoCAR	-1.233	0.286	-4.318	1.58E-05
ns(Day, df = 5)1:GroupCD70 nanoCAR - MGAT5 KO	-0.038	0.455	-0.084	0.932877
ns(Day, df = 5)2:GroupCD70 nanoCAR - MGAT5 KO	-2.329	0.504	-4.619	3.86E-06
ns(Day, df = 5)3:GroupCD70 nanoCAR - MGAT5 KO	-2.697	0.390	-6.909	4.89E-12
ns(Day, df = 5)4:GroupCD70 nanoCAR - MGAT5 KO	-2.689	0.817	-3.289	0.001005
ns(Day, df = 5)5:GroupCD70 nanoCAR - MGAT5 KO	-3.019	0.304	-9.940	2.8E-23
Random intercept S.D. (ID=mouse)	0.675			

B

Contrast	Estimate	95% CI, lower	95% CI, upper	Adj. p-value
Ratio of CD70 nanoCAR over MGAT5 KO CD70 nanoCAR tumor sizes at day7	0.994	0.432	2.291	1
Ratio of CD70 nanoCAR over MGAT5 KO CD70 nanoCAR tumor sizes at day 77	6.366	3.152	12.857	<0.001

Secondary Tumor (Donor C)

C

Parameter	estimate	std.error	statistic	p.value
(Intercept)	2.653	0.944	2.809	0.004965
ns(Day, df = 3)1	0.931	0.281	3.309	0.000936
ns(Day, df = 3)2	1.652	0.570	2.895	0.003791
ns(Day, df = 3)3	1.507	0.198	7.623	2.47E-14
GroupCD70 nanoCAR	-1.036	2.005	-0.517	0.60516
GroupCD70 nanoCAR - MGAT5 KO	-0.309	1.327	-0.233	0.81609
ns(Day, df = 3)1:GroupCD70 nanoCAR	-0.310	0.704	-0.440	0.659863
ns(Day, df = 3)2:GroupCD70 nanoCAR	0.062	1.359	0.045	0.963834
ns(Day, df = 3)3:GroupCD70 nanoCAR	-0.344	0.489	-0.704	0.481702
ns(Day, df = 3)1:GroupCD70 nanoCAR - MGAT5 KO	-0.141	0.427	-0.331	0.740974
ns(Day, df = 3)2:GroupCD70 nanoCAR - MGAT5 KO	-0.564	0.832	-0.677	0.49826
ns(Day, df = 3)3:GroupCD70 nanoCAR - MGAT5 KO	-0.404	0.305	-1.325	0.185164
Random intercept S.D. (ID=mouse)	2.787			

D

Contrast	Estimate	95% CI, lower	95% CI, upper	Adj. p-value
Ratio of CD70 nanoCAR vs MGAT5 KO CD70 nanoCAR tumor sizes at day 98	0.483	0.007	31.857	0.824
Ratio of CD70 nanoCAR vs MGAT5 KO CD70 nanoCAR tumor sizes at day 119	0.675	0.011	40.483	0.936

1343 **Supplementary Figure 6 | Longitudinal analysis of Donor C.** Longitudinal analysis of the primary (A-B) and
1344 secondary tumor (C-D). A Tweedie GLMM (generalized linear mixed model) with log link was used to model
1345 the tumor volume. **A and C**. Summary of the model output, listing all parameter estimates for the model
1346 TumorVol ~ ns(Day, df = 5)*Group + (Day | ID), ns = natural spline. The table gives parameters and standard
1347 errors on the natural log scale together with test statistics and multiple testing adjusted p-values (null
1348 hypothesis: parameter equal to zero). **B and D**. Inference for different research questions. In this table, the
1349 estimates and confidence intervals are transformed back to the original scale so we can interpret them in
1350 a straightforward way. S.E.: Standard Error. CI: Confidence Interval.

1351

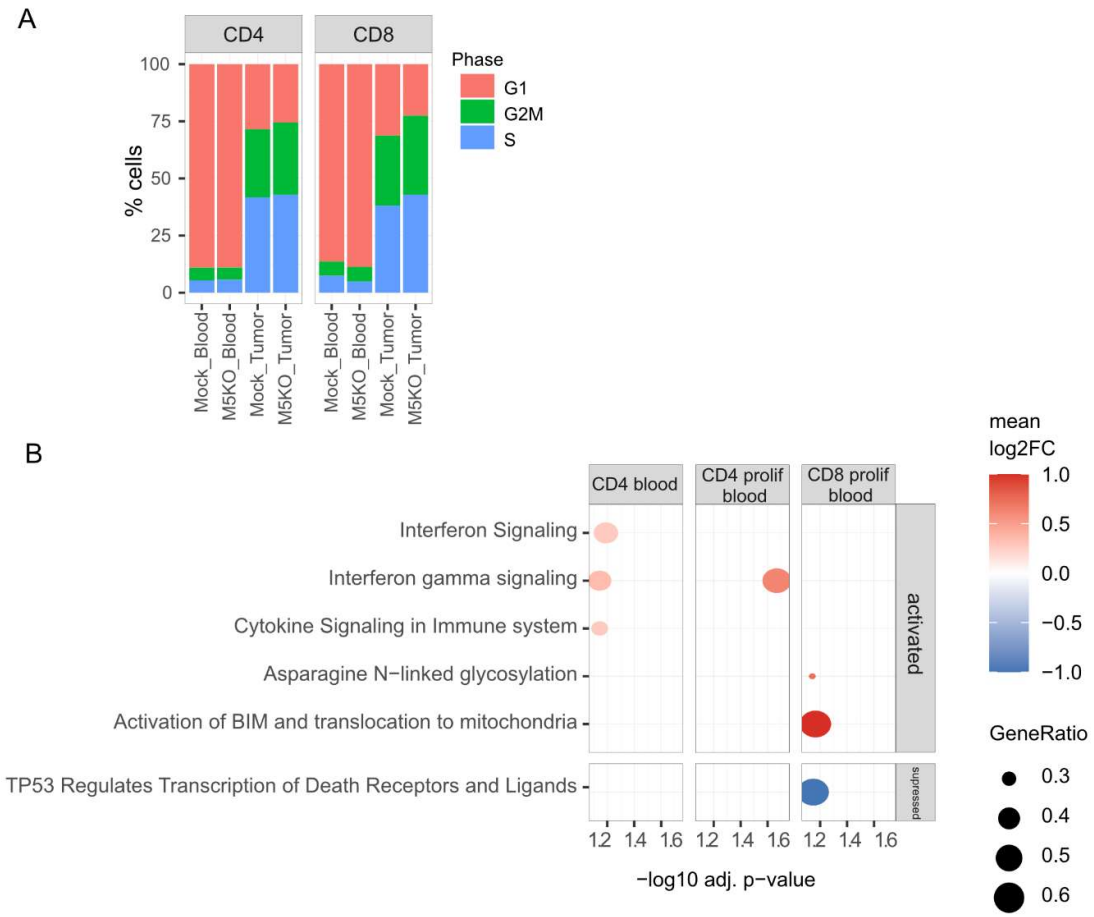

Supplementary Figure 7| Single cell RNA sequencing of tumor-infiltrating and circulating CAR T cells. A. Both $CD4^+$ and $CD8^+$ subpopulations of MGAT5 KO CD70 nanoCAR T cells infiltrating the tumor showed a higher proportion of proliferating cells (G2M and S phase). **B.** Gene set enrichment analysis of Reactome pathways for $CD4^+$ and $CD8^+$ MGAT5 KO CD70 nanoCAR T cells circulating in blood.

1357 **Supplementary Tables**

1358 **Supplementary Table 1**– List of differentially expressed genes in nanoCAR T cells from the 7 different
1359 clusters

1360 Attached as separate file

1361

1362 **Supplementary Table 2-** Output of the Gene set enrichment analysis of Reactome pathways from the 7
1363 different clusters

1364 Attached as separate file

1365

1366 Supplementary Table 3– Overview of the different donors used in this study

Donor	Experiment type in which T cells were used	
A	*in vivo* analysis tumor control efficacy SKOV-3 model	
B	*in vivo* analysis tumor control efficacy SKOV-3 model	
C	*in vivo* analysis tumor control efficacy SKOV-3 model	
D	*in vivo* analysis tumor control efficacy Raji model	
E	*in vivo* analysis tumor control efficacy Raji model	
F	*in vivo* analysis tumor control efficacy Raji model	
G	*in vivo* analysis tumor control efficacy Raji model	Cytokine-independent growth assay
H	analysis *ex vivo* tumor cell killing activity	
I	analysis *ex vivo* tumor cell killing activity	
J	scRNA seq experiment	
K	degranulation assay	

1367

1368 Supplementary Table 4– Overview of antibodies used in this study

Channel ID	Target	Clone	Fluorochrome	Dilution (x)	Company	Cat N°
B530	GFP					
B710	CD45	HI30	PerCP-Cy5.5	20	BD Biosciences	564105
V525	CD3	UCHT1	BV510	40	Biolegend	300447
V605	CD25	BC96	BV605	80	Biolegend	302631
R730	CD4	RPA-T4	AF700	40	BD Pharmingen	561030
R780	Viability		eFL780	1000	eBioscience	65-0865-18
Y586	Nanobody	96A3F5	iFluor555	200	Genscript	A01863
Y610	CD279 (PD-1)	EH12.2H7	PE/Dazzle594	80	Biolegend	329939
Y780	CD69	FN50	PE-Cy7	80	Biolegend	310911
UV379	CD62L	SK11	BUV395	10	BD Biosciences	565219
UV735	CD45RA	HI100	BUV737	80	BD Biosciences	612846
UV810	CD8	SK1	BUV805	40	BD Biosciences	612889
Y586	CD70	113-16	PE	10	Biolegend	355104
B710	CD70	113-16	PerCp-Cy5.5	80	Biolegend	355107
V710	IFNg	4S.B3	BV711	20	Biolegend	502539
Y586	IL-2	MQ1-17H12	PE	20	Biolegend	500306
UV379	TNFa	MAb11	BUV395	20	BD horizon	563996
UV379	CD107	H4A3	BUV395	20	BD Biosciences	565113

1369